이학박사학위논문

Scalable Transfer and Production of Graphene for Industrial Applications

산업 응용 가능한 그래핀 대면적 전사 및 대량 생산에 관한 연구

2016 년 8 월

서울대학교 대학원

화학부 물리화학 전공

최 태 준

Scalable Transfer and Production of Graphene for Industrial Applications

산업 응용 가능한 그래핀 대면적 전사 및 대량 생산에 관한 연구

지도교수: 홍 병 희

이 논문을 이학박사 학위논문으로 제출함

2016년 7월

서울대학교 대학원

화학부 물리화학전공

최태준

최태준의 이학박사 학위논문을 인준함

2016년 6월

위 원 장 장 두 전 ㊞

부위원장 홍 병 희 ㊞

위 원 이 연 ㊞

위 원 조 성 표 ㊞

위 원 김 선 국 ㊞

Ph. D. Thesis

Scalable Transfer and Production of Graphene for Industrial Applications

Supervisor: Professor Byung Hee Hong

Major: Physical Chemistry

By Taejun Choi

Department of Chemistry

Graduate School of Seoul National University

2014

Abstract

Emerging electronics including bendable and rollable displays, and flexible sensors come closer to reality by showing the feasibility of industrial-level production of high quality graphene sheets by Chemical Vapor Deposition (CVD). However, transferring on the desired substrate and patterning for graphene device fabrication are still limited. The quality degradation is evitable during transferred on a desired flexible substrate, which is mainly incurred by the chemical damage and residues on removal of the support layer such as PMMA and the thermal damage by the use of a Thermal Release Tape (TRT). As for patterning, existing methods including lithographical methods and plasma etching are costly and hardly scalable as well as require complicated pre-defined masking and wet chemical etching processes.

Here we present a roll-to-roll patterning and transfer of graphene sheets capable of residue-free, no chemical treatment, and fast patterning. The graphene sheet attached to a Pressure Sensitive Film (PSF) is continuously patterned by applying pressure selectively with the pre-defined embossed roll. The patterned graphene sheet is adhered to the PSF with very low strength and can be easily transferred to the curved surface or a variety of flexible substrate without the aid of any heating mechanism. Compared to the transfer by the TRT and the PMMA support, the reduction in the occurrence of debris and defects was verified through Raman spectroscopy.

In the other hands, exfoliation based methods are useful for the large scale production of graphene platelets and for low-end products, e.g., fillers for polymer composites, electrode materials for battery and supercapacitor, conductive inks and

coatings etc. because of its unique combination of very high strength and stiffness, and excellent electrical and thermal conductivities. These applications require huge quantities of graphene in the form of nanosheets, nanoparticles or nanoplatelets at a reasonable cost; however, purity is not the major issue in this case. As a solution, the mechanical exfoliation by the air jet mill is demonstrated, which is very effective and easy to scale up for any industrial application. The proposed method is especially useful for a layered material such as graphite having low interfacial bonding energy between layers so that the layer can be easily exfoliated by the mechanical forces. The raw graphite flakes of average 800 microns in diameter immediately had size reduction to few microns in average diameter within few minutes, which is advantageous considering typical exfoliation method such as ball milling take few tens hours of operation time. During the process, the fragmentation by collision is observed to be more dominant than the exfoliation by shear and normal forces. It is not usually desirable, but small flakes obtained from the air jet mill can enhance the exfoliation efficiency with the help of intercalation agents or further process with minimum amount of chemical promoter. Formation of bonds with undesirable oxygen species kept low up to only few percent even after few successive air jet mill runs, assuming that the defects on the basal plane would not be produced much during the process.

Keywords: Graphene, Transfer, Patterning, Large Scale, Mass Production, Jet Milling

Student Number: 2013-30095

Scope and Format of Dissertation

The dissertation is divided into three research chapters. Chapter 1 describe the problems to commercialize the graphene material and the current advances in producing graphene, which are categorized into two groups, i.e. top-down methods and bottom-up methods. In Chapter2, a roll-to-roll, continuous patterning and transfer of graphene sheets are presented, which is capable of residue-free and fast patterning. The graphene sheet is supported with dispersive adhesion. In Chapter 3, we propose a high efficient, low cost exfoliation method of graphite to produce graphene using an air jet milling. The compressed air flows generate a vortex to give the graphite flakes directional shear so that the flakes are exfoliated efficiently.

Contents

List of Figures

514nm). b, The G and 2D band shift of graphene. The G and 2D band peaks of graphene samples transferred using PMMA and TRT are relatively red-shifted compared to one done by PSAF. c, XPS spectra of graphene transferred by PSAFs, PMMA and TRT film, respectively. d, The current-gate voltage curves of the graphene FETs measured at V_{SD}= 10 mV. The inset illustrates structure of FETs device. (channel width : 50um, channel length :250um)

Figure 3. The transfer and patterning of the graphene using PSAFs. a,b, Large scale graphene transferred on the 4" wafer (a) and PET (b). (scale bar = 2cm) c, The transferred graphene on non-flat vial surface using PSAFs. (scale bar = 1cm) d, The simple electrical measurement (LED on-off) of graphene, inset shows that light on image. Graphene utilized as an electrical pathway. e,f, Patterned graphene on SiO_2/Si substrate using PSAFs and stamping mask. (scale bar = 100um)

Figure 4. The sheet resistance and transmittance of monolayer graphene with respect to the number of PSAF recycle. a, Sheet resistance of monolayer graphene. b, Transmittance of monolayer graphene. There are no significant degradation of transferred graphene qualities.

Figure 5. Schematic illustration of roll-to-roll continuous patterning and transfer. a, The process flow. In the magnified figures, the size of arrows represent the strength of adhesion force at the interface. b, Calculations of surface energy and adhesion force with a single layer graphene from the contact angle measurements. Δ represents the difference of adhesion forces between each substrate interface and the silicone interface, that is, $W_{SLG/Sub}$-$W_{SLG/Silicone}$.

Figure 6. Pre-patterned embossing roller and detailed view of pattern. a, Four bands of patterns (120 mm width) and the magnified view of university mark pattern. b, 3D profile of leaf shape on university mark. c, The scan of the depth profile (~ 15μm).

Figure 7. Patterning and characterization. a, Roll patterning with the embossed roll (120 mm width). b, Transfer of patterned graphene and optical image of school mark onto SiO_2/Si. The dark areas show graphene. The scale bars is 500 μm. c, Detailed views from SEM images. d, Raman spectrum of single spots for removed and remained area. 2D/G ratio is 2.5 and FWHM is 31.5 cm^{-1}. e, Raman spectrum of single spots for removed and remained area. 2D/G ratio is 2.5 and FWHM is 31.5 cm^{-1}.

Figure S1. Pressure dependence on the transfer quality of graphene. The pressure values on the arrow mark represent the applied pressure by the patterned roller. Higher pressing pressure of the patterned roller guarantees conformal contacts between the roller and results in the distinct pattern. The scale bars are 300 μm.

Figure S2. The ATR-FTIR spectrum of the silicone used as the adhesive layer. The Si-CH_3 group is recognized by a sharp band at about 1260 cm^{-1} together with more strong bands in the range 865-789 cm^{-1}. Some long or branched siloxane (Si-O-Si) chains are identified by the broad and complex bands in the range of 1110-1010 cm^{-1}.

Figure S3. SEM images of residual graphene on the patterning roller. a, SEM images. Dark and bright areas represent the graphene residues and bare surface of the patterned mask respectively. The scale bars are 500 μm and 200 μm respectively. b,

c, Raman spectra and Raman mapping image of G peaks near the boundary of two areas. Relatively high D peaks imply possible cracks and damages due to high pressure by the roller, which, however, to be removed eventually.

Chapter 3

Figure 1. The schematics of exfoliation of graphite using the air jet milling. a, The conceptual structure of air jet milling machine. The compressed air is applied in the tangential direction of the milling zone, and the raw graphite is put from the top of the milling zone. The final exfoliated graphene or graphite flakes are obtained from the top and bottom bottles. b, The side view of the milling zone. Small flakes enough to stay in the middle escape from the milling zone through the discharge port.

Figure 2. The mechanism of exfoliation and fragmentation of the graphite flakes inside the milling zone. a, The normal force is generated by the centrifugal force and the centripetal force exerted on the graphite flakes and the shear force is given by the compressed air flow between the graphite layers. b, By the balance between the centrifugal force and the centripetal force, the graphite flakes are sorted by the size and weight from the wall to the center of the mill. c, The collisions among the graphite flakes promote the fragmentation of the flakes.

Figure 3. The appearance of the air jet milling machine and its components. a, The overall view of the machine. The magnified view of its major components are shown separately from b to e. b, The milling zone, where the compressed air are forced into the zone through the nozzles. c, The top view inside the milling zone. d, The material feeder. e, The collecting bottle.

Figure 4. The changes in size and its distribution after three cycle runs of air jet mill. a, The profile of size distribution is represented as a hatched closed curve. Thin and thick meshed curves show the distribution of the flakes obtained from the top bottle and the bottom bottle respectively. b, SEM images of raw graphite and after each cycle are shown, where the stage is distinguished with alphabets.

Figure 5. The FT-IR analysis and XPS analysis for oxygen concentration. a, FT-IR analysis shows the dominant functional groups for the samples from each cycle. b, C 1s spectra of XPS analysis. c, carbon and oxygen concentration of the air jet milled samples and GO calculated from XPS data.

Figure 6. The Raman Analysis of the Jet Milled Samples and the Graphene Oxide by typical Hummer's methods. a, Raman peaks of jet milled samples. D peaks and the shift of G peaks. All the peaks are normalized by the intensity of G peak. b, Raman peaks of GO samples.

Figure S1. AFM analysis showing the morphology of the flakes. a, Graphite flakes from 1st cycle (Top bottle). b, Graphite flakes from 2nd cycle (Top bottle). c, Graphite flakes from 3rd cycle (Top bottle).

Figure S2. XPS data. a-e, C 1s and O 1s peaks from pristine graphite, 1st cycle, 2nd cycle, 3rd cycle, and Graphene oxide respectively.

List of Tables

Chapter 1

General Introduction

1.1 Historical Backgrounds

The existence of graphene was predicted by physicists over 40 years ago but it was not until 2004 when Geim and Novoselov of Manchester University successfully isolated single layer of graphite for the first time using a commercial Scotch tapes.[1] Previously the general belief was that graphene cannot maintain its 2D structure in the natural environment and it is thermodynamically unstable with low melting point. However the discovered graphene was very stable and had high crystallinity.

Since then, graphene has been intensively studied and its outstanding properties were discovered. Some of them are the record high as shown in Fig. 1. The intrinsic mobility of graphene at room temperature (RT) was expected to be 2 x 10^5 cm^2 V^{-1} s^{-1}, higher than any known semiconductor as described in Fig. 1a.[2] Despite the remote interfacial phonon (RIP) scattering by the polar optical phonons of the SiO_2 substrate, graphene on SiO_2 showed a room-temperature mobility of 4 x 10^4 cm^2 V^{-1} s^{-1}, which is comparable with the best InAs and InSb field-effect transistors (FETs). Graphene also has an outstanding thermal properties as shown in Fig. 1b. The thermal conductivity of large-area suspended single-layer graphene (SLG) is experimentally measured to be in the range between 3,000 and 5,000 $Wm^{-1}K^{-1}$ near room temperature, which is clearly above the bulk graphite limit, that is, 2,000 $Wm^{-1}K^{-1}$.[3] The upper bound thermal conductivity for graphene was obtained for the largest SLG flakes examined (~20 μm x 5 μm). As in Fig 1c, the mechanical properties of SLG is also demonstrated, where the free-standing graphene film was

indented at the center of the film with an AFM cantilevers with diamond tips.[4] A Young's modulus of 1 TPa and an intrinsic strength of 130 GPa were obtained for the SLG from all data, which corresponds to more than 200 times than that of steel. The atomic thick SLG has a high transmittance of ~97.7% as shown in Fig. 1d so that it can be a strong candidate for transparent and flexible electrode material.

These unique properties make graphene a key candidate material for many applications such as electronic devices, flexible display, energy devices, advanced composites, barrier materials, ink, heat spreader, bio related applications, etc. as described in Fig. 2. However, despite its outstanding properties, key applications of graphene are not commercially notable up to now. One of the greatest challenges being faced in commercializing graphene is how to produce high quality material, on a large scale at low cost, and in a reproducible manner. A large number of methods have been proposed to produce graphene as described in Fig. 3. This method can be divided into two main classes, that is, bottom-up methods and top-down methods. The former depends on the chemical reaction of the molecules to form a covalent bonded two dimensional structure. The typical examples are chemical vapor deposition (CVD) and epitaxial growth on SiC substrates. The latter depends on the separation of the bulk graphite. By considering the production cost (expandability to mass production) and output material quality as described in Fig. 3, they can again be grouped to three domains as described. Among those methods, two major production methods, i.e. CVD based method and exfoliation based methods are handled in this study since they are believed to be suitable for mass production of graphene.

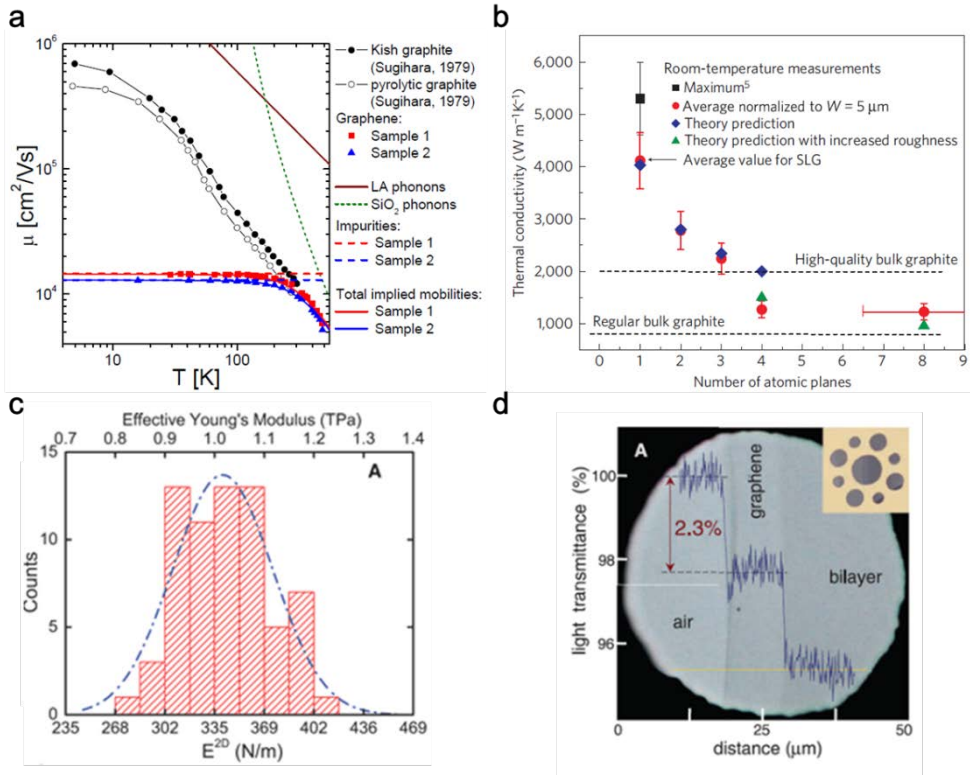

Figure 1. Outstanding Properties of Graphene a, The temperature-dependent mobilities of graphene and graphite. Adapted from Ref. 2. **b**, Measured thermal conductivity as a function of the number of atomic planes in FLG. Adapted from Ref. 3. **c**, Histogram of elastic stiffness of suspended graphene obtained from elastic response test results. Adapted from Ref. 4. **d**, Photograph of a 50-mm aperture partially covered by graphene and its bilayer. Adapted from Ref. 5.

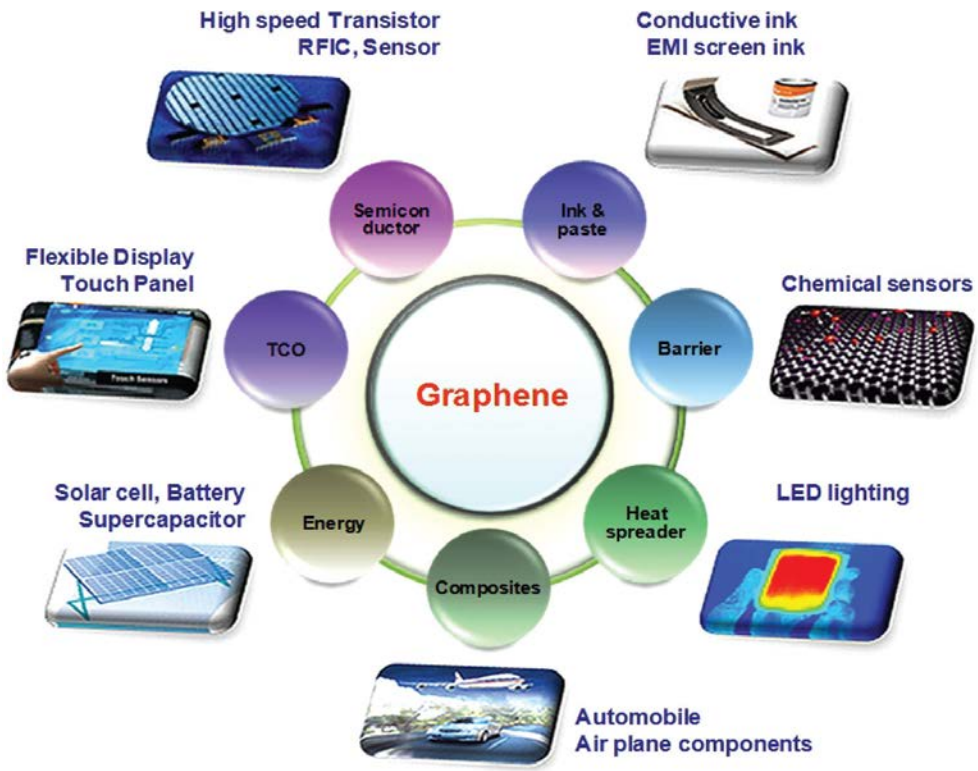

Figure 2. Overview of Applications of Graphene in different sectors ranging from conductive ink to chemical sensors, light emitting devices, composites, energy, touch panels and high frequency electronics. Adapted from Ref. 6.

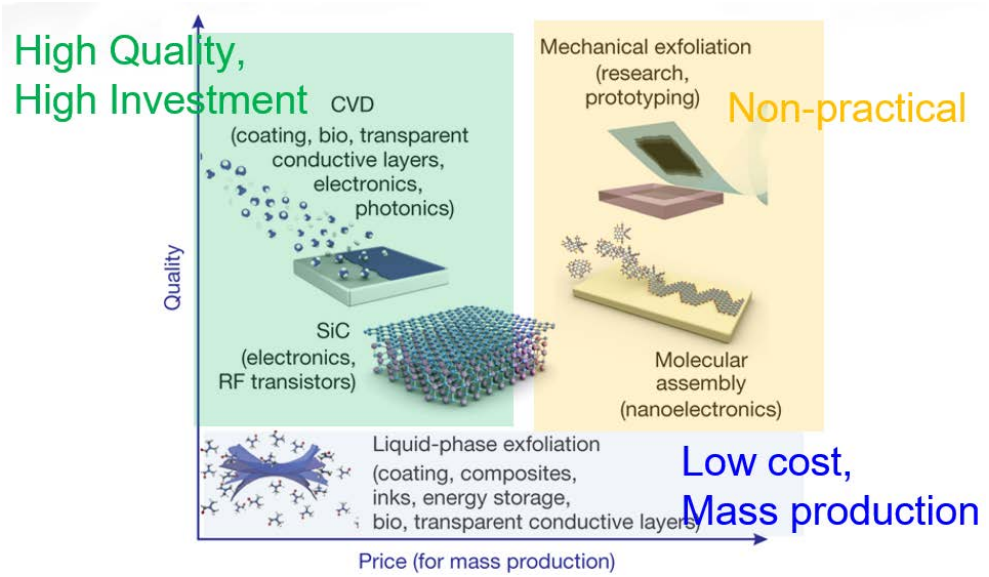

Figure 3. Various Methods for Mass-production of Graphene in terms of size, quality and price for any particular application. Adapted from Ref. 7.

1.2 Chemical Vapor Deposition (CVD) Synthesis of Graphene

Graphene is an ideal candidate for the manufacture of the next generation lightweight, ultra-fast and high frequency electronic and optoelectronic devices. The quality of the graphene is of great importance for these applications and for this purpose one has to produce large area graphene monolayer or few layer thin films of ultimate purity, large domain size, and uniform thickness. Moreover, the material should be free of any defects, grain boundaries, structural disorder, and wrinkles. The CVD approach has the potential to produce graphene thin films to meet these strict requirements. The other requirement is that one should be able to produce it on a large scale by adopting continuous production process.[8]

For the CVD approach, transferring graphene to a target substrate without residue or defects is of a great importance as much as synthesizing high quality graphene. To protect graphene from cracks and defects during the transfer process, different types of polymer films have been utilized as the graphene supporting layer. Namely, the poly methyl methacrylate (PMMA) layer coated on graphene/ catalyst has been used for standard (wet) and bubble transfer. Another supporting polymer such as the thermal release tape (TRT) has been utilized to transfer the graphene on large scale arbitrary substrates to support the graphene layer.[9] However, these polymer-based transfer methods have remnant residue problem. Moreover, TRT transfer method requires a high temperature process to release graphene, which induces thermal stress on both graphene and the target substrates. Metal supporting transfer methods such as TEM grid or deposited metal layer are not suitable

processes to obtain large scale graphene. Although other various polymer coating or annealing methods were employed to obtain clean graphene surface, these strategies accompanied additional cleaning processes.

In order to employ graphene for various applications, graphene patterning is also an essential process. However, most patterning methods such as photolithography or E-beam lithography cause polymer residues, which results in unwanted doping effects on the graphene. Other materials supported patterning such as block copolymer or inorganic material guided patterning methods have a relatively long patterning time and scale-up limitation problem. Thus, simple and residue-free patterning method has been demanded to obtain clean graphene surface in cost efficient manner.

1.3 Exfoliation-based Methods

Exfoliation based methods are useful for the large scale production of graphene nano platelets and for low-end products, e.g., fillers for polymer composites, electrode materials for battery and supercapacitor, conductive inks and coatings etc. because of its unique combination of very high strength and stiffness, and excellent electrical and thermal conductivities. These applications require huge quantities of graphene in the form of nanosheets, nanoparticles or nanoplatelets at a reasonable cost; however, purity is not the major issue in this case. Therefore, economically viable processes for its mass production have to be developed.

Among various methods, chemical reduction of Graphene Oxide (GO) seems to be the most promising route because it enables large-scale production of functionalized graphene at low-cost. However, GO synthesized by Hummer’s or

modified Hummer's methods requires use of strong and hazardous oxidizers such as sulphuric acid, potassium permanganate, and etc. Moreover, the reduced graphene film is prepared by subjecting GO to chemical treatments using highly toxic and unstable hydrazine, which requires utmost care.

To overcome the chemical exfoliation method by GO, many mechanical exfoliation based methods are recently proposed including the exfoliation by ball milling processes and the shear based exfoliation method by fluid dynamics. Among many mechanical exfoliation methods, a ball milling can be a promising candidate for the scalable production of graphene, which uses shear forces to exfoliate graphite flakes. Recently, Jeon et al. suggested an edge functionalized dry ball milling. They dry milled the pristine graphite flakes in for 48 hours in the presence of dry ice, homogenous but much smaller edge-carboxylated graphite grains of the few hundreds nanometer size can be obtained.[10] They claimed the edge-carboxylated graphite is highly dispersible in various solvents and can self-exfoliate into mono and few-layer graphene nanosheets. However, the fragmentation and defects are inevitable during the milling process since high energy collisions among the grinding media cannot be prevented and the long process time of several ten hours increase the possibility of generating defects.

Besides the above discussed ball milling, the exfoliation methods by the shear force generated from fluid dynamics have a good potential for producing graphene.[11] Graphite flakes can move with the liquid or air flow in a circular container and the centrifugal forces are exerted on the graphene flakes in the opposite direction of drag force by liquid or air flow. Therefore, the flakes experience a shear

induced displacement along the wall of the container and are exfoliated efficiently. This mechanism is intrinsically different from that of ball milling in that the fluid dynamics based methods generate directional shear forces by the flow unlike the ball milling uses random directional shear forces and impact forces.

1.4 References

[1] K. S. Novoselov, A. K. Geim, S. Morozov, D. Jiang, Y. Zhang, S. Dubonos, I. Grigorieva and A. Firsov, *Science*, **2004**, 306, 666–669.

[2] J.-H. Chen, C. Jang, S. Xiao, M. Ishigami, M. S. Fuhrer, *Nature Nanotechnol*. **2008**, 3 (4), 206–209.

[3] S. Ghosh,W. Bao, D. L. Nika, S. Subrina, E. P. Pokatilov, C. N. Lau and A. A. Balandin1, *Nature Materials.*, **2010**, 9, 555-558.

[4] C. Lee, X. Wei, J. W. Kysar and J. Hone, *Science*, **2008**, 321, 385–388.

[5] R. R. Nair, P. Blake, A. N. Grigorenko, K. S. Novoselov, T. J. Booth, T. Stauber, N. M. R. Peres and A. K. Geim, *Science*, **2008**, 320, 1308–1308.

[6] A. C. Ferrari et. al., *Nanoscale*, **2015**, 7, 4598

[7] K. S. Novoselov, V. I. Fal'ko, L. Colombo, P. R. Gellert, M. G. Schwab, and K. Kim, *Nature*, **2012**, 490, 192-200.

[8] K. S. Kim, Y. Zhao, H. Jang, S. Y. Lee, J. M. Kim, K. S. Kim, J. H. Ahn, P. Kim, J. Y. Choi, and B. H. Hong, *Nature*, **2009**, 457, 706-710.

[9] S. Bae, H. Kim, Y. Lee, X. F. Xu, J. S. Park, Y. Zheng, J. Balakrishnan, T. Lei, H. R. Kim, Y. I. Song, Y. J. Kim, K. S. Kim, B. Ozyilmaz, J. H. Ahn, B. H. Hong, and S. Iijima,, *Nature Nanotechnology*, **2010**, 5, 574-578.

[10] I. Y. Jeon, Y. R. Shin, G. J. Sohn, H. J. Choi, S. Y. Bae, J. Mahmood, S. M. Jung, J. M. Seo, M. J. Kim, D. Wook Chang, L. Dai and J. B. Baek, *Proc. Natl. Acad. Sci. U. S. A.*, **2012**, 109, 5588–5593.

[11] K. R. Paton, E. Varrla, C. Backes, R. J. Smith, U. Khan, A. O'Neill, C. Boland,

M. Lotya, O. M. Istrate, P. King, T. Higgins, S. Barwich, P. May, P. Puczkarski, I. Ahmed, M. Moebius, H. Pettersson, E. Long, J. Coelho, S. E. O'Brien, E. K. McGuire, B. M. Sanchez, G. S. Duesberg, N. McEvoy, T. J. Pennycook, C. Downing, A. Crossley, V. Nicolosi and J. N. Coleman, *Nat. Mater.*, **2014**, 13, 624–630.

Chapter 2

Roll-to-roll Continuous Patterning and Transfer of Graphene via Dispersive Adhesion

2.1 Introduction

Graphene has been intensively studied due to their outstanding electrical, mechanical and optical properties, such as high electrical conductivity, mechanical flexibility, and optical transmittance[1]. The key challenges to make commercially viable graphene-based electronic devices are enabling large-area production of high quality graphene and subsequently patterning graphene into desirable structures. In recent years, researchers have endeavored to obtain a high quality of large-scale graphene by modifying growth the conditions of chemical vapor deposition (CVD). With the recent advances in chemical vapor deposition (CVD), large-area growth of graphene by CVD on Cu substrates was successfully demonstrated for industrial applications[2,3]. However, reliable methods are still required to transfer the large-area graphene sheet to the application substrate[4,5] and pattern for the desired applications[6] without damaging or leaving undesired residues on the graphene surface. As for the graphene transfer, the wet transfer method using a support layer such as poly(methyl methacrylate) (PMMA)[7] is typically used but generally difficult to scale up, and the surface tension experienced by the floating graphene at the air-water interface causes rippling, rolling, and break of the films during transfer. The complete removal of PMMA residues is also problematic and most of flexible substrates are either dissolved in acetone or cannot withstand the annealing temperature; thus, graphene can only be transferred to a limited number of flexible substrates. On the other hands, the transfer method using a thermal release tape (TRT) is easy to transfer large-area graphene onto flexible or rigid substrates[8,9], but inevitably contaminates the

transferred graphene with the adhesive from the TRT film. The adhesion of polymer supports (i.e., PMMA and TRT) to the graphene mainly depends on the chemical adhesion of the polymer film. The residual PMMA or adhesive left on the graphene surface is inevitable. Unlike the adhesive-based transfer mechanism such as PMMA or TRT, a dispersive adhesion-based transfer methods[10] have been demonstrated including the work by Allen, M. J. *et. al.*[11] using a soft PDMS stamp[12,13,14]. The transfer mechanism there was based on the difference in dispersive adhesion at the PDMS-graphene and graphene-substrate interfaces. For most materials, the PDMS interface is weaker than the substrate interface, due to the extremely low surface energy of PDMS. Nevertheless, their transfer method required contact time of several days to fully transfer. As a result, residues of low molecular weight oligomers from the PDMS stamp remained on the graphene surface, which were dissociated from the surface of the stamp over time. To overcome the problem, Chen, X. D. *et. al.* [15] suggested a two-layer structure of polyethylene terephthalate (PET) and silicone, where the PET layer works for the mechanical support and the silicone layer provides dispersive adhesion. In fact, a two-layer structure film for the roll-to-roll transfer of graphene was first reported using commercial ethylene-vinyl acetate copolymer (EVA) coated PET sheets[16], where the viscosity of EVA layer played a role of laminating EVA/PET layer onto few-layer graphene (FLG) grown on the Ni foil with heating and then detaching the FLG from the Ni surface on cooling. However, the EVA/PET film required heating and was not reusable unlike the PET/silicone film. The concept was similar in that the silicone has as much low surface energy as PDMS, but the strong self-adhesive characteristics of the silicone

enabled graphene to adhere and release instantly without leaving any noticeable residue on graphene surface. Another obstacle lies in that complicated patterning processes are still required to fabricate the desired shapes, even after graphene is successfully transferred onto the desired substrate. For example, lithographic methods such as conventional photolithography[17], electron beam lithography[18], and ion beam lithography[19] have been widely used to produce graphene patterns for electronic devices but undergo the issues including low throughput and multiple processing steps which hamper the large-area and roll-to-roll fabrication of graphene-based devices. Laser direct wring[20] is a one-step, clean process without using any chemical, but the thermal damage generated by heat is usually unavoidable. An ultra-short pulsed laser such as femto-second laser can relieve this problem, but is not suitable and costly for large-scale production.

Here we report a simple and novel graphene patterning and transferring technique using pressure sensitive adhesive films (PSAF) at the room temperature that can be utilized to fabricate graphene devices with outstanding properties. This simple transfer method is caused by the adhesion energy difference between PSAF and target substrates. To prove that the PSAF-graphene exhibits superior properties, graphene was transferred on the SiO_2 / silicon substrate using various polymer films including PSAF, PMMA and TRT. Through the measurements of the Raman band shift, sheet resistance and the Dirac voltage shift of field effect transistors (FETs) device, it was confirmed that the graphene transferred using the PSAF had the least amount of polymer residue on the surface – which was further visualized through optical microscopy (OM) and atomic force microscopy (AFM) images. In addition,

graphene was patterned simply by mask stamping method. We recycle the PSAF up to four times and could not find any noticeable changes in graphene. Besides the outstanding experimental results, the recyclability of PSAF is notable; environmentally friendly transfer process is thus suggested for the first time. We also present a roll-to-roll continuous patterning and transfer methods applicable to various substrates using the PSAF. Pattern and transfer can be continuously performed without requiring any additional complex system and the method is fitted to the roll-to-roll large-scale production.

2.2 Experimental

Graphene was synthesized through the chemical vapor deposition method on a high purity copper catalyst under H_2 condition (70 mtorr) with CH_4 gas source (650 mtorr). As-grown graphene on copper catalyst was attached to PSAF by roll to roll process and the copper catalyst was subsequently etched in ammonium persulfate (APS) solution. After several rinsing processes in distilled water, graphene on PSAF was stored in dehydrated condition. Figure 1 shows the simple transfer and patterning processes of graphene using PSAF. Following the adhesion step between graphene on PSAF and a desired substrate (i.e. silicon wafer or polyethylene terephthalate (PET)), slowly releasing the PSAF allows transferred graphene on the flat or round target substrate (Fig. 1c). Figure 1d,f show the schematics of graphene using simple stamping mask and transferring of patterned graphene on rigid wafer substrates. Pressure sensitive adhesive solution are prepared by mixture of silicon based adhesives which have low adhesion property. It shows wet-out performance to various target materials such as PET or glass and adhere well through it has very lower adhesive force. We confirmed that PSAF is consisted of silicone adhesive polymer spread on PET films. Graphene layer was easily transferred to target substrates such as quartz or glass owing to the fact that the adhesion energy between graphene and silicon is weaker than it is the oxide layer. It was found that the adsorption of graphene on the O-polar surface is stronger than that on the Si-polar surface. The charge transfer effect of O-polar surface increases the electrostatic interaction between graphene and oxidized surface.

Figure 2a shows the Raman spectra of graphene transferred on the substrates (Si/SiO_2 wafer) using various polymer films. From the negligibly small D peak and the intensity ratio between the G band and the 2D band, we could confirm that high quality monolayer graphene was obtained. Although the intensity ratios between the G band and the 2D band are similar

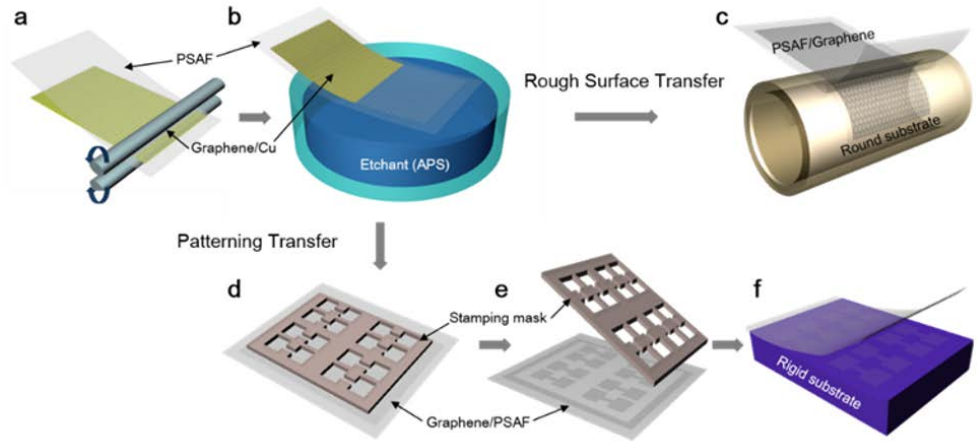

Figure 1. The schematics of the graphene pattering and transfer processes using PSAFs. **a,b,** PSAFs coating process. **a,** The graphene and copper foil coated with PSAFs by R2R method. **b,** The Cu catalyst etched by APS etchant. **c-f,** graphene pattering and transfer on various substrates at room temperature condition. **c,** The graphene transferred on non-flat substrates. **d,f,** The graphene was directly patterned by stamping mask and transferred on rigid substrate.

regardless of the type of polymer film, the positions of the 2D band differed for each film. The Raman band shifts with various supporting films show in Figure 2b.

The G band peaks of graphene samples transferred using PMMA (~1584 ± 1.5 cm^{-1}) and TRT (~1585 ± 1.0 cm^{-1}) are relatively blue shifted compared to the one done by PSAF (~1583 ± 1.5 cm^{-1}). In addition, while the 2D band peak for the PSAF graphene is located around 2688 ± 3.8 cm^{-1}, the same band peaks for PMMA and TRT graphene are found around 2697cm^{-1} on average, showing they were also relatively more p-doped. From these results, it can be inferred that the PSAF induces the least doping effect.[1] Such varying degree of p-doping effect was most likely derived from remained polymer residue during transfer process which could be further confirmed from the device results. Figure 2c shows the X-ray photoelectron spectroscopy (XPS) spectra of PSAF, PMMA and TRT transfer method, respectively. The C1s spectrum of graphene using PSAF and PMMA have relatively narrow bandwidth (centered peak at 285.2 $\pm$ 0.03 eV) than TRT method. The spectra of PMMA and TRT methods show a slight band shift with chemical effect from remnant residues than of PSAF. The atomic force microscopy (AFM) mapping images also show that the transferred graphene using PSAF has clean surface and less residue than graphene transferred by PMMA and TRT (Supplementary Fig.1). To measure the electric properties of the individual graphene samples, FETs with source and drain electrodes were fabricated. The I-V transport curves show that PMMA (V_{Dirac}= +40V) and TRT (V_{Dirac}= +113V) graphene FETs exhibit more p-doping than PSAF

(V_{Dirac}= +3V) (Table 1 and Fig. 2d). Moreover, the field effect mobility of PSAF graphene (4206 $cm^2 V^{-1} s^{-1}$) was larger than those of PMMA and TRT graphene. Dry transfer methods can prevent induced water trap between graphene and substrates during the wet transfer processes. Such outcome implies that incompletely removed residue on the graphene surface not only affects the Dirac voltage but also causes carrier scattering, which eventually decreases the carrier mobility.

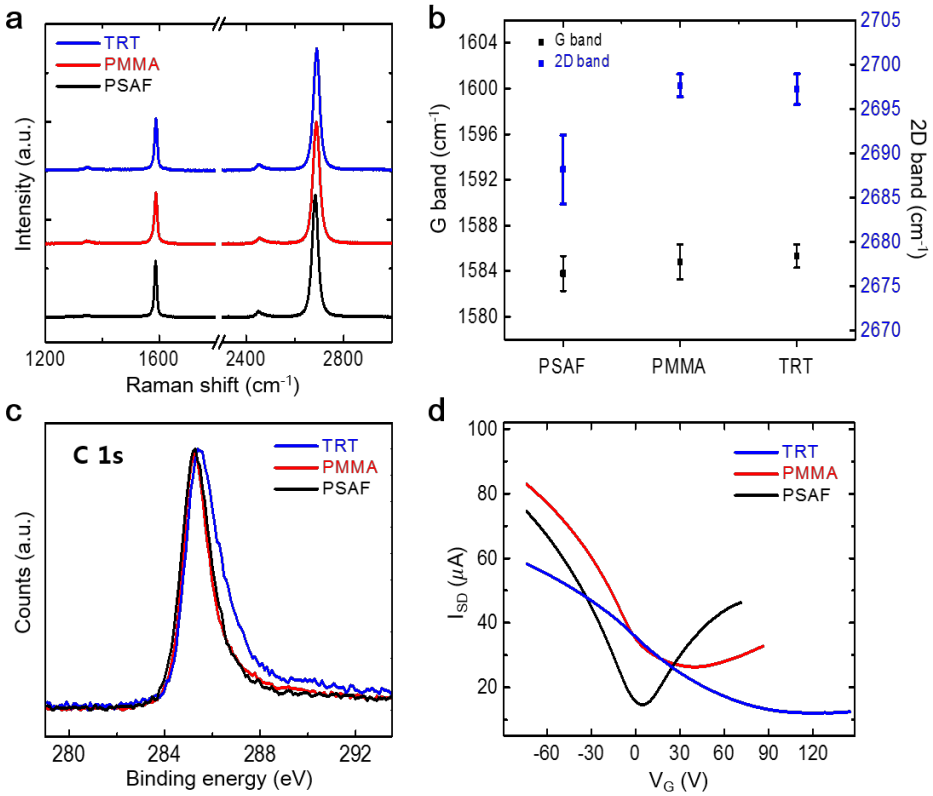

Figure 2. The graphene transferred using various supporting polymers. a, Raman spectra of graphene transferred on SiO_2/Si substrate (excitation wavenumber: 514nm). **b,** The G and 2D band shift of graphene. The G and 2D band peaks of graphene samples transferred using PMMA and TRT are relatively red-shifted compared to one done by PSAF. **c,** XPS spectra of graphene transferred by PSAFs, PMMA and TRT film, respectively. **d,** The current-gate voltage curves of the graphene FETs measured at V_{SD}= 10 mV. The inset illustrates structure of FETs device. (channel width : 50um, channel length :250um)

Table 1. The Dirac voltage value and carrier mobility respectively for different supporting films.

	PSAF	**PMMA**	**TRT**
Dirac voltage (V)	+ 3	+ 40	+ 113
Electron mobility ($cm^2/V·s$)	4206	3549	1584
Hole mobility ($cm^2/V·s$)	2834	1374	393

Figure 3 shows the optical images of transferred or patterned graphene on various substrates using PSAF. The large-scale graphene are successfully transferred onto 4-inch Si wafer and PET. (Fig. 3a,b) We also conducted a simple circuit measurement of LED device with graphene transferred on a non-flat vial surface as electrical pathway (Fig. 1c,d). The optical microscopy (OM) images of well patterned graphene using PSAF and stamping mask is shown in Supplementary Fig. 2a and Figure 3e,f. We confirmed that different patterns of graphene were fabricated using different stamping masks. In addition, only insignificant amount of residue was remained on the graphene surface transferred on the polyimide (PI) substrate by roll to roll transfer method (Supplementary Fig. 2b). The G and 2D peak Raman mapping images of patterned graphene (dashed area in Supplementary Fig. 2a)) using stamping mask (patterning transfer), well patterned graphene edge image are confirmed in the Raman mapping images (Supplementary Fig. 2c,d).

As shown in Figure 4, the recyclability of PSAFs for graphene transfer was tested. Figure 4 shows the sheet resistance and the transmittance of graphene as a function of recycle times, ranging from one to four times of reuse. The obtained values, ~97.5% and ~400 ohm/sq, respectively for the transmittance and the sheet resistance, of monolayer graphene were relatively unchanged as a function of recycling times. Such result indicates that recycling PSAF has no significant effect on graphene transfer process; the use of PSAF can be deemed environmentally friendly. On the other hand, TRT cannot be recycled once in use after transfer process and environmentally harmful organic solvent is required to remove PMMA film. The Supplementary Fig. 3 shows the sheet resistance mapping of large-scale monolayer

graphene transferred on PET film. The sheet resistance of graphene treated with dopant, H_2SO_4 and H_2O_2 based etchant was 250 ohm/sq. on average with the the surface area of approximately 80×120 mm^2.[i] The uniform sheet resistance suggests that there is no significant defect on the surface;

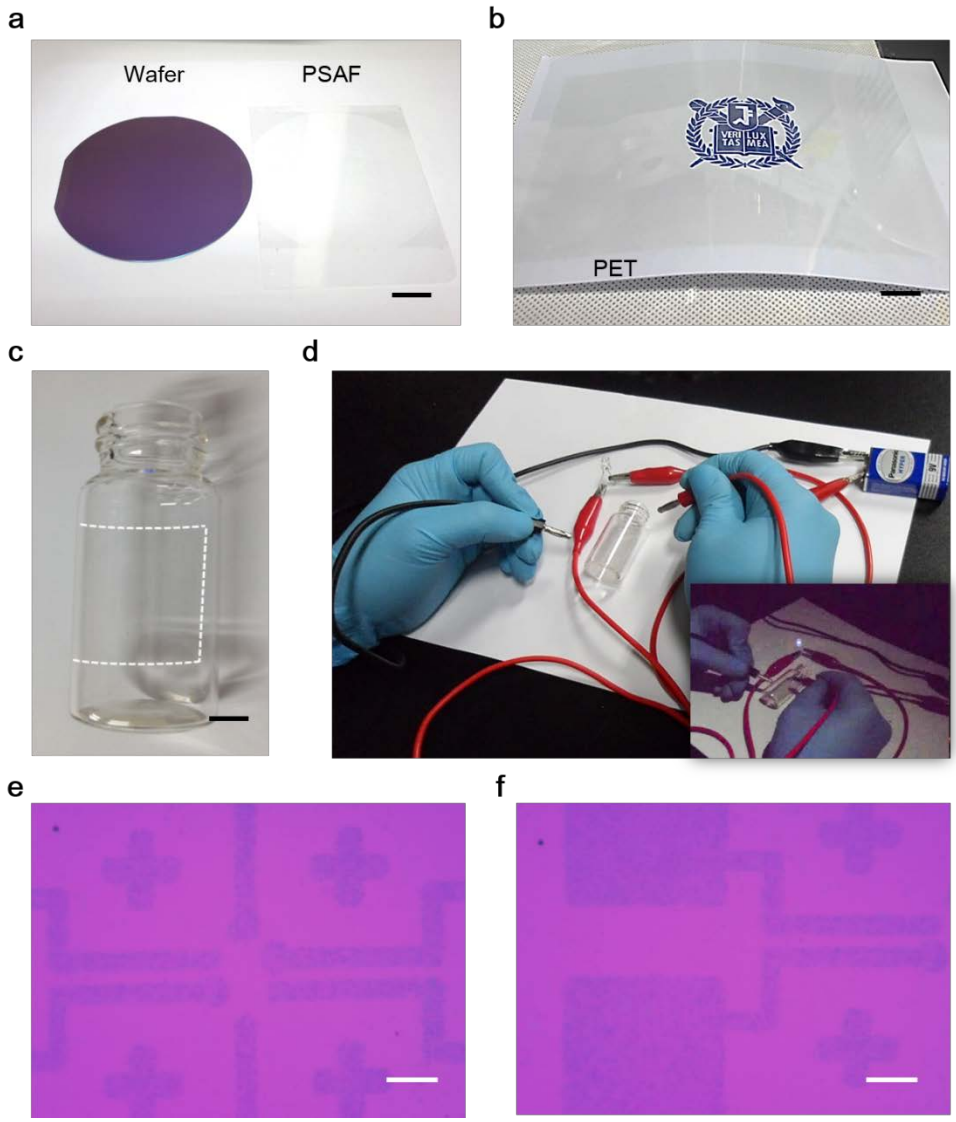

Figure 3. The transfer and patterning of the graphene using PSAFs. a,b, Large scale graphene transferred on the 4" wafer **(a)** and PET **(b)**. (scale bar = 2cm) **c,** The transferred graphene on non-flat vial surface using PSAFs. (scale bar = 1cm) **d,** The simple electrical measurement (LED on-off) of graphene, inset shows that light on image. Graphene utilized as an electrical pathway. **e,f,** Patterned graphene on SiO_2/Si substrate using PSAFs and stamping mask. (scale bar = 100um)

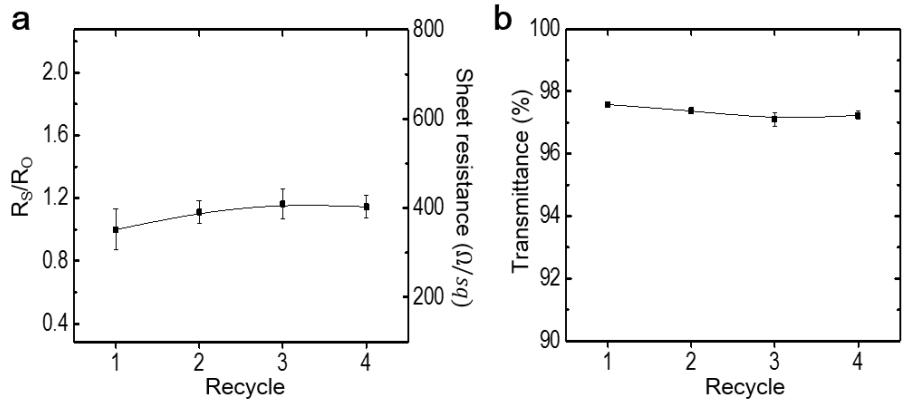

Figure 2. The sheet resistance and transmittance of monolayer graphene with respect to the number of PSAF recycle. a, Sheet resistance of monolayer graphene. **b,** Transmittance of monolayer graphene. There are no significant degradation of transferred graphene qualities.

PSAF can be used as a supporting film that guarantees high quality graphene without much residue and defects.

The process was extended to a roll-to-roll patterning and transferring processes, described as in Figure 5a, where the CVD-grown monolayer graphene on a copper foil is attached to a low adhesion PET/silicone by passing together between two rollers while forming a conformal contact. For the PET/silicone layer, a commercial screen protector film (Befind BF-D503A for iPad Air) is used. The Attenuated Total Reflection Flourier Transformed Infrared (ATR-FTIR) spectrum of the silicone (see Fig. S2) shows that the silicone contains long and branched siloxane (Si-O-Si) chains and Si-CH_3 groups[21]. In the subsequent step, the copper layer is removed with aqueous 0.1 M ammonium persulphate solution $(NH_4)_2S_2O_8$[22,23], and the desired patterns are imprinted on the graphene film when the PET/silicone/graphene film is pressed between the embossed roller with reverse patterns and a backup roller. PET/silicone/graphene layer contacts only with the embossed parts of the roller and is deformed vertically due to the applied pressure so that dislocation would occur at the edges between the contacted and non-contacted parts resulting in tailoring graphene at the edges of the roller. The departed contacted parts of graphene attach to the surface of the patterning roller due to high adhesion force at the interface and the rest of graphene remains on the PET/silicone layer. Cracks on graphene can be observed on the surface of the patterning roller, which are, however, to be removed eventually (see Fig. S3), but graphene on the PET/silicone will remain free of cracks. Finally, the graphene film with the desired patterns is easily transferred from the PET/silicone film onto a target substrate by the difference in adhesion forces

between graphene/silicone and graphene/target substrate. The mechanisms are mainly governed by the difference of work of adhesion involved in the surface energy of each layer. In order to pattern graphene, the work of adhesion at the graphene and the surface of reversely patterned roller should be higher than that at the silicone and graphene interface. Similarly, graphene can be transferred onto a target substrate when the work of adhesion with the target substrate is higher than that with silicone. The surface tension of the silicone can be calculated from the following equation as in Chen, X.-D.[15]:

$$(1+\cos\theta)\gamma_L = 2\left\{\left(\gamma_L^d\gamma_S^d\right)^{1/2} + \left(\gamma_L^p\gamma_S^p\right)^{1/2}\right\} \quad (1)$$

, where θ is the contact angle of a test liquid on the silicone, γ_L and γ_S are the surface energy of the test liquid and the solid surface, and the superscripts *d* and *p* represent dispersion and polar component respectively. To determine two unknowns in Eq. (1), γ_S^d and γ_S^p , water and Methylene iodide were used as testing liquids[24]. Once the surface energy is determined for the solid surface, the work of adhesion at the layer 1 and 2 is given by:

$$W_{12} = 4\left(\frac{\gamma_1^d\gamma_2^d}{\gamma_L^d+\gamma_L^d} + \frac{\gamma_1^p\gamma_2^p}{\gamma_L^p+\gamma_L^p}\right) \quad (2)$$

Since the silicone has very low surface energy of 16.4 mJ/m^2, which is calculated as shown in Figure 5b, the adhesion force between silicone and graphene is much smaller than that between graphene and most of substrates. Thus the graphene can be attached to the embossed surface of the roller on patterning and released the target

substrates on transfer successfully. The magnified illustration in Figure 5a shows the balance of the adhesion energies at the interface, where the size of arrows represents the strength of adhesion forces. On a basis of atomic force, the attraction force of PET/silicone with graphene is weak but can still become significant when summed over the bulk of the silicone layer and graphene. So the graphene will be intact and not separated from the silicone layer during the transfer process.

To fabricate the patterned roller, an AISI 1045 carbon steel cylinder with the diameter of 100 mm and the length of 550 mm was engraved by 1064nm (30 nsec) pulsed laser at a density of 40.7 J/cm^2 at room temperature (RT) in air. Four different test patterns including

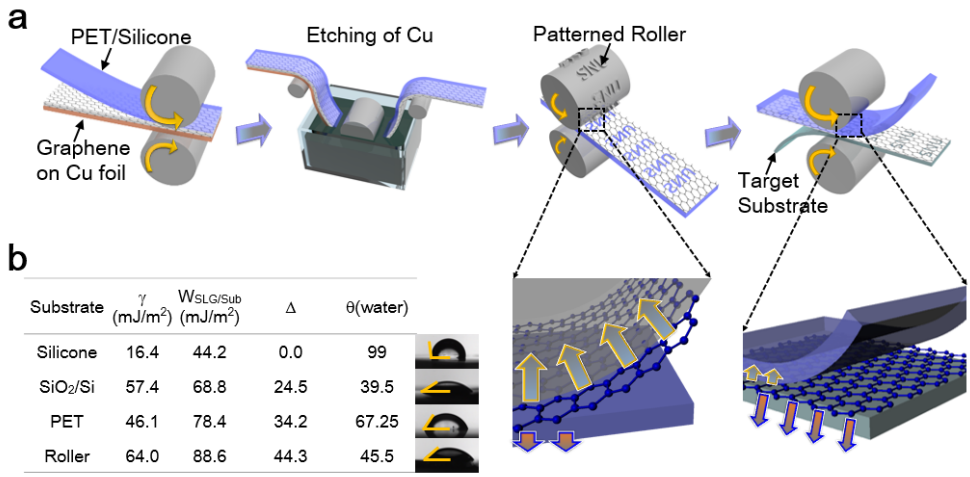

Substrate	γ (mJ/m^2)	$W_{SLG/Sub}$ (mJ/m^2)	Δ	θ(water)
Silicone	16.4	44.2	0.0	99
SiO_2/Si	57.4	68.8	24.5	39.5
PET	46.1	78.4	34.2	67.25
Roller	64.0	88.6	44.3	45.5

Figure 5. Schematic illustration of roll-to-roll continuous patterning and transfer. a, The process flow. In the magnified figures, the size of arrows represent the strength of adhesion force at the interface. **b,** Calculations of surface energy and adhesion force with a single layer graphene from the contact angle measurements. Δ represents the difference of adhesion forces between each substrate interface and the silicone interface, that is, $W_{SLG/Sub}$-$W_{SLG/Silicone}$.

university marks, texts, vertical lines with the width of 40 μm, and squares with sides of 50 μm were prepared with the depths of approximately 15 μm as shown in Figure 6. Arrays of the repeated patterns were arranged with the width of 30 mm per pattern, which summing up to the total pattern width of 120 mm.

After the patterns are engraved by the nano-second pulsed laser, mechanical polishing was applied using a cylindrical polishing machine to achieve the surface roughness of 0.02 μm in RMS value. The smooth roller surface helps the roller to make a conformal contact with the graphene surface on patterning. The measured optical profile as in Figure 6c also confirms the smoothness of the top surface though the bottoms of the patterns are rough due to the melting and recast processes of laser ablation. However, the bottom surfaces does not directly contact with the graphene surface on patterning and affect any quality of patterning.

As shown in Figure 7a, the graphene/silicone/PET film (50 x 100 mm^2) was patterned by passing between the embossed roller and the backup roller using a commercial roll-to-roll embossing machine. The embossed roller rotated at a high speed of 15 m/min and the applied pressure was 0.1 MPa. After the graphene/silicone/PET film is patterned, it can be transferred onto any desired substrate such as PET and SiO_2 wafer. The patterned film was then attached onto 4 inch SiO_2/Si wafer with dispersive adhesion. Finally, the PET/silicone film was peeled off instantly since the adhesion force between the PET/silicone and the graphene is much lower than that between the SiO_2/Si wafer and the graphene as calculated in Figure 5b.

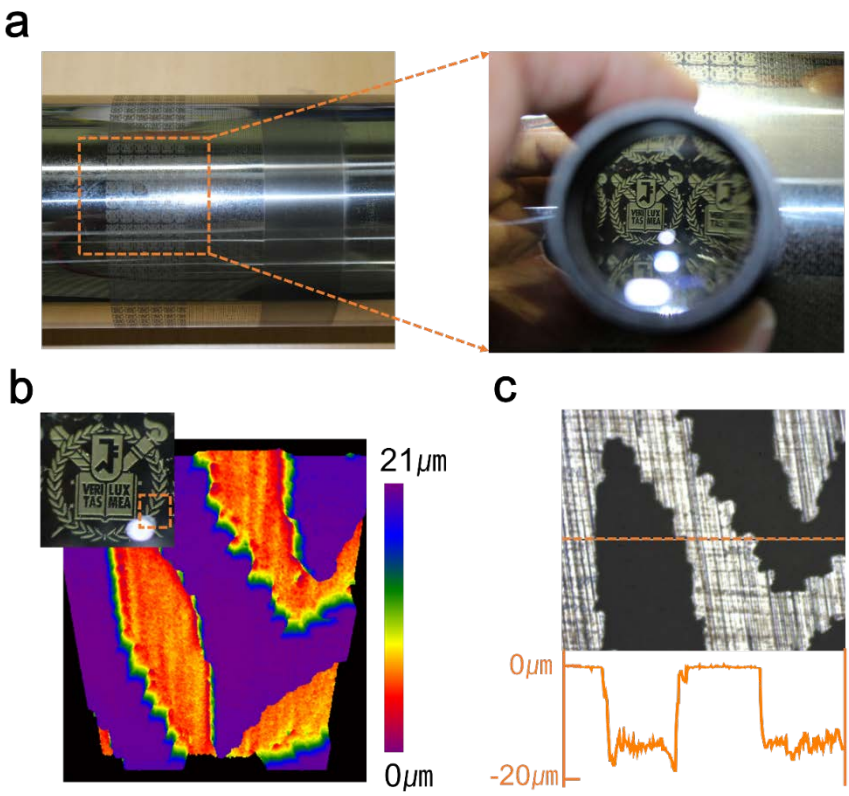

Figure 6. Pre-patterned embossing roller and detailed view of pattern. a, Four bands of patterns (120 mm width) and the magnified view of university mark pattern. **b,** 3D profile of leaf shape on university mark. **c,** The scan of the depth profile (~ 15μm).

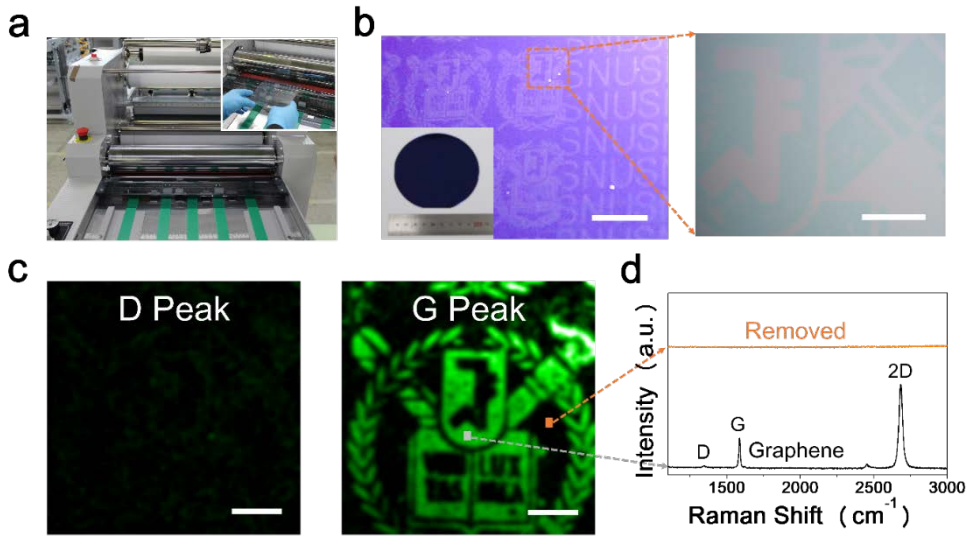

Figure 7. Patterning and characterization. a, Roll patterning with the embossed roll (120 mm width). **b,** Transfer of patterned graphene and optical image of school mark onto SiO_2/Si. The dark areas show graphene. The scale bars is 500 μm. **c,** Detailed views from SEM images. **d,** Raman spectrum of single spots for removed and remained area. 2D/G ratio is 2.5 and FWHM is 31.5 cm^{-1}. **e,** Raman spectrum of single spots for removed and remained area. 2D/G ratio is 2.5 and FWHM is 31.5 cm^{-1}.

2.3 Results and Discussion

The surface morphology of patterned and transferred graphene on SiO2/Si wafer was investigated by optical microscopy and scanning electron microscopy (SEM) as in Figure 7b and 7c. Clear distinction was made between the mono-layered graphene area (dark) and the removed area (bright). Especially, the uniformity of patterns can be observed in the large area as in Figure 7b. The quality of patterned graphene films was further analyzed by Raman spectroscopy. Figure 7e shows the Raman spectra of spots from the mono-layer graphene area (black) and the removed area (red) using Renishaw Raman system equipped with a 514 nm laser source and 50x objective lens. The G peak (1588 cm^{-1}) of the graphene Raman spectrum corresponds to the doubly degenerate E2g phonon at the Brillouin zone center, whereas the D peak (1357 cm^{-1}) is caused by the breathing mode of sp^2 rings and is activated by the existence of defects. The defect-related D-band of the monolayer graphene transferred by the roller is almost negligible. A symmetric 2D band centered at 2650 cm^{-1} has a full width at half maximum (FWHM) of 31.5 cm^{-1}, and the corresponding intensity ratio of I_{2D}/I_G is approximately 2.5. All of these Raman spectroscopy results are consistent with those of high-quality monolayer graphene reported in the literatures. To check the quality and uniformity of the patterns, the Raman mapping images of large-area pattern were also obtained using Witec 300R Raman system with a 532 nm laser source. The measured size was 5 x 5 mm^2, which covered a whole pattern of one school mark. The sample was moved with a rough step size of 40 μm, and the crisp distinction between the removed area and the graphene area

was observed from the G peak mapping image for the large pattern area, and the intensity of the G peaks in the mapping image is also uniform for the entire area. The mapping image for D peak around 1357 cm^{-1} showed negligible intensities.

2.4 Conclusions

In summary, we have demonstrated a simple graphene patterning and transfer technique using PSAF at room temperature that can be utilized to fabricate large scale graphene with outstanding properties. The simple process is possible to transfer the graphene easily owing to adhesion energy difference of PSAF and target substrates. We compared the individual graphene transferred on the substrates using various polymer films including PSAF, PMMA and TRT. Through the measurements of Raman spectroscopy and FETs devices, it was confirmed that the graphene transferred using PSAF had the least amount of polymer residue and showed the least doping effects. In addition, patterned graphene was simply fabricated by mask stamping, it can be utilized on roll to roll process for mass production. Moreover, the fact that the PSAF can be recycled is notable for its environmentally friendly process. It can be utilized for protection film of graphene to preserve the graphene until its usage.

We also developed an efficient method for continuous patterning and transfer large-scale graphene. The method is easy to combine with roll-to-roll processes for industrial applications. The two layer structure of the PSAF use dispersive adhesion so that fast patterning and transfer is possible and meets the industrial requirements for the roll-to-roll continuous production. Furthermore, due to the low surface energy of silicone, the graphene showed clean and uniform surface after patterning and transferring. Continuous patterning and transferring of a large-scale graphene with the size of 120 mm were demonstrated with various patterns and showed high quality,

which was verified with optical microscopy, Raman spectra, and large-area Raman mapping.

2.5 Methods

Graphene synthesis and transfer process. Graphene was synthesized by chemical vapor deposition (CVD) method on a high purity copper foil with flowing 3 sccm H_2 and 30 sccm CH_4 gases at 1,000^{o}C. After coating a PSAF, TRT and PMMA polymer layers on one side of as-grown Cu foil, the graphene on the other side was removed by several water spraying during the etching process. The ammonium persulfate (APS) and benzimidazole(BI) mixed acidic solution were used for Cu catalyst etching. After rinsing with distilled water, the graphene was transferred on target substrates. Polymers were individually removed by simple attach and detach (PSAF), heat source (TRT), acetone treatment (PMMA), respectively.

PSAF preparation. Pressure sensitive adhesive (PSA) consisted with mixture of silicone based adhesive solutions (Dow corning). The PSAs were made by mixture of DOW CORNING® 7646 ADHESIVE : DOW CORNING® 7652 ADHESIVE : toluene with a mass ratio of 1: 1: 2. After stirred for 5 hours, additionally, SYL-OFF® SL 7028 CROSSLINKER and SYL-OFF® SL 9250 ANCHORAGE ADDITIVE were added in the mixture (mass ratio of 1 : 200), respectively. Additionally, SYL-OFF® 4000 CATALYST added in total mixture and stirred 1hour. Finally, PSA solution were spin-coated on the PET substrates (4000 rpm, 30sec) and basked at 150 ^{o}C for 1 min.

Characterization. The AFM image was measured by a noncontact mode (Park System, XE-100). XPS analyses were carried out using Thermo Scientific K-Alpha (small-spot X-ray Photoelectron Spectrometer system). The Raman spectra were obtained by a Raman spectrometer (RM 1000-Invia, Renishaw, 514nm). The optical transmittance of graphene was measured using an ultraviolet-visible spectrometer (UV-3600, Shimazdu). The sheet resistance was measured with 4-point probe nanovoltmeter (Keithley 6221), and the current-voltage curve was measured by Agilent B2912A.

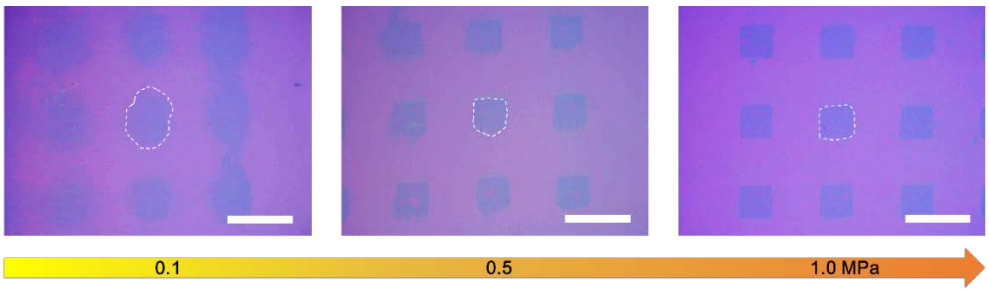

Figure S1. Pressure dependence on the transfer quality of graphene. The pressure values on the arrow mark represent the applied pressure by the patterned roller. Higher pressing pressure of the patterned roller guarantees conformal contacts between the roller and results in the distinct pattern. The scale bars are 300 μm.

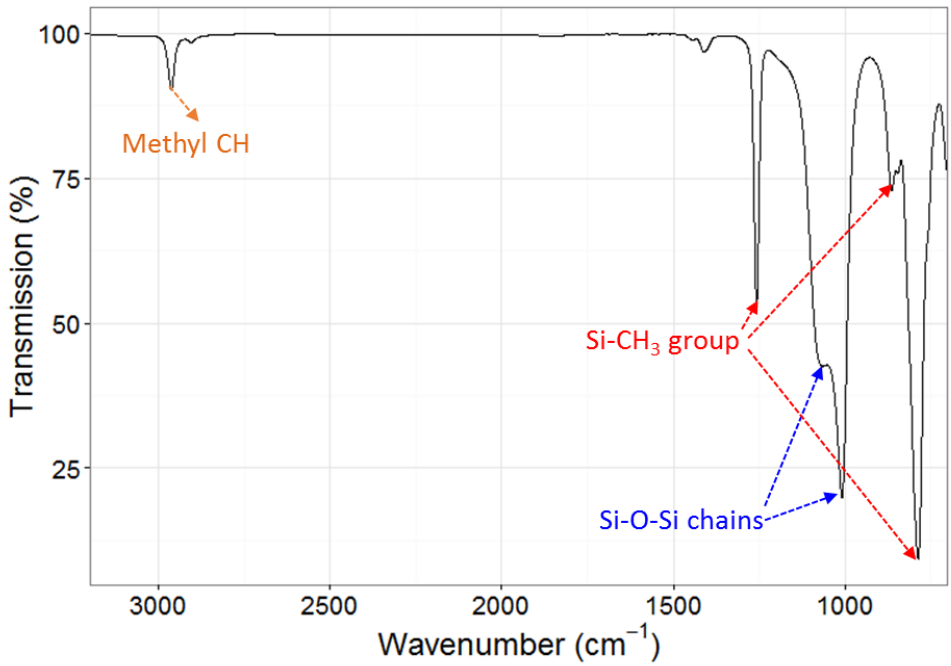

Figure S2. The ATR-FTIR spectrum of the silicone used as the adhesive layer. The $Si\text{-}CH_3$ group is recognized by a sharp band at about 1260 cm^{-1} together with more strong bands in the range 865-789 cm^{-1}. Some long or branched siloxane (Si-O-Si) chains are identified by the broad and complex bands in the range of 1110-1010 cm^{-1}.

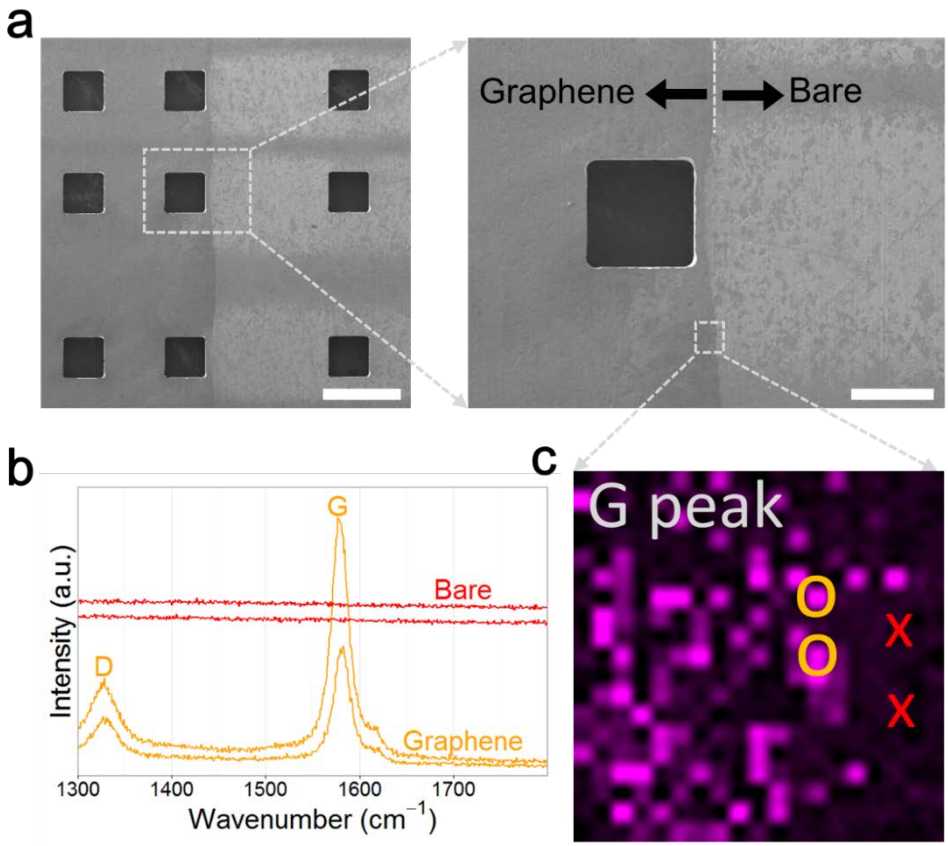

Figure S3. SEM images of residual graphene on the patterning roller. a, SEM images. Dark and bright areas represent the graphene residues and bare surface of the patterned mask respectively. The scale bars are 500 μm and 200 μ m respectively. **b, c,** Raman spectra and Raman mapping image of G peaks near the boundary of two areas. Relatively high D peaks imply possible cracks and damages due to high pressure by the roller, which, however, to be removed eventually.

2.6 References

[1] A. K. Geim and K. S. Novoselov, *Nature Materials*, **2007**, 6, 183-191.

[2] K. S. Kim, Y. Zhao, H. Jang, S. Y. Lee, J. M. Kim, K. S. Kim, J. H. Ahn, P. Kim, J. Y. Choi, and B. H. Hong, *Nature*, **2009**, 457, 706-710.

[3] J. Ha, S. Park, D. Kim, J. Ryu, C. Lee, B. H. Hong and Y. Hong, *Organic Electronics*, **2013**, 14, 2324-2330.

[4] Y. Lee, S. Bae, H. Jang, S. Jang, S. E. Zhu, S. H. Sim, Y. I. Song, B. H. Hong, and J. H. Ahn, *Nano Letters*, **2010**, 10, 490-493.

[5] L. Gao, G. X. Ni, Y. Liu, B. Liu, A. H. Castro Neto, and K. P. Loh, *Nature*, **2014**, 505, 190-194.

[6] Y. Zhou and K. P. Loh, *Advanced Materials*, **2010**, 22, 3615-3620.

[7] Xuesong Li, Yanwu Zhu, Weiwei Cai, Mark Borysiak, Boyang Han, David Chen, Richard D. Piner, Luigi Colombo, and Rodney S. Ruoff, *Nano Letters*, **2009,** 9, 4359-4363.

[8] S. Bae, H. Kim, Y. Lee, X. F. Xu, J. S. Park, Y. Zheng, J. Balakrishnan, T. Lei, H. R. Kim, Y. I. Song, Y. J. Kim, K. S. Kim, B. Ozyilmaz, J. H. Ahn, B. H. Hong, and S. Iijima,, *Nature Nanotechnology*, **2010**, 5, 574-578.

[9] J. Kang, S. Hwang, J. H. Kim, M. H. Kim, J. Ryu, S. J. Seo, B. H. Hong, M. K. Kim, and J. B. Choi, *ACS Nano*, **2012**, 6, 5360-5365.

[10] J. Song, F. Y. Kam, R. Q. Png, W. L. Seah, J. M. Zhuo, G. K. Lim, P. K. Ho, and L. L. Chua, *Nature Nanotechnology*, **2013**, 8, 356-362.

[11] Matthew J. Allen, Vincent C. Tung, Lewis Gomez, Zheng Xu, Li-Min Chen, Kurt S. Nelson, Chongwu Zhou, Richard B. Kaner, and Yang Yang, *Advanced Materials*, **2009**, 21, 2098-2102.

[12] Matthew A. Meitl, Zheng-Tao Zhu, Vipan Kumar, Keon Jae Lee, Xue Feng, Yonggang Y. Huang, Ilesanmi Adesida, Ralph G. Nuzzo, and John A. Rogers, *Nature Materials*, **2005**, 5, 33-38.

[13] Y. Q. Bie, Y. B. Zhou, Z. M. Liao, K. Yan, S. Liu, Q. Zhao, S. Kumar, H. C. Wu, G. S. Duesberg, G. L. Cross, J. Xu, H. Peng, Z. Liu, and D. P. Yu, *Advanced Materials*, **2011**, 23, 3938-3943.

[14] S. Y. Yang, A. Carlson, H. Cheng, Q. Yu, N. Ahmed, J. Wu, S. Kim, M. Sitti, P. M. Ferreira, Y. Huang, and J. A. Rogers, *Advanced Materials*, **2012**, 24, 2117-2122.

[15] X. D. Chen, Z. B. Liu, C. Y. Zheng, F. Xing, X. Q. Yan, Y. Chen, and J. G. Tian, *Carbon*, **2013**, 56, 271-278.

[16] Z. Y. Juang, C. Y. Wu, A. Y. Lu, C. Y. Su, K. C. Leou, F. R. Chen and C. H. Tsai, *Carbon*, **2010**, 48, 3169-3174.

[17] C. H. Liu, Y. C. Chang, T. B. Norris, and Z. Zhong, *Nature Nanotechnology*, **2014**, 9, 273-278.

[18] C. O. Girit, J. C. Meyer, R. Erni, M. D. Rossell, C. Kisielowski, L. Yang, C. H. Park, M. F. Crommie, M. L. Cohen, S. G. Louie, and A. Zettl, *Science*, **2009**, 323, 1705-1708.

[19] M. C. Lemme, D. C. Bell, J. R. Williams, L. A. Stern, B. W. H. Baugher, P. Jarillo-Herrero, and C. M. Marcus, *ACS Nano*, **2009**, 3, 2674-2676.

[20] J. H. Yoo, J. B. Park, S. Ahn, and C. P. Grigoropoulos, *Small*, **2013**, 9, 4269-4275.

[21] D. R. Anderson, Analysis of silicones, Wiley-Interscience, New York, **1974**.

[22] J. Park, S. Park, S. Ryu, S. H. Bhang, J. Kim, J.-K. Yoon, Y. H. Park, S.-P. Cho, S. Lee, B. H. Hong and B.-S. Kim, *Advanced Healthcare Materials*, **2014**, 3, 176-181.

[23] T. J. Lee, S. Park, S. H. Bhang, J. K. Yoon, I. Jo, G. J. Jeong, B. H. Hong and B. S. Kim, *Biochemical and Biophysical Research Communications*, **2014**, 452, 174-180.

[24] F. M. Fowkes, F. L. Riddle Jr, W. E. Pastore and A. A. Weber, *Colloids and Surfaces*, **1990**, 43, 367-387.

Chapter 3

High Effective and Economical Mechanical Exfoliation of Graphite via Jet Milling

3.1 Introduction

Graphene as a kind of two dimensional nanomaterial has attracted worldwide attention since its discovery in 2004[1], and has been one of the hottest material studied due to its outstanding properties, where some of them are the record high including a Young's modulus of 1 TPa, an intrinsic strength of 130 GPa, a high electron mobility at room temperature (RT) of 2.5 x 10^5 cm^2 V^{-1} s^{-1} [3], a high electron mobility at 4 K of ~6x10^6 cm^2 V^{-1} s^{-1}, a high thermal conductivity of ~2000 to 5300 W m^{-1} K^{-1}, a high current densities several million times larger than that in copper, and so on.[2-6] Graphene also shows extremely high resistance to gas permeation, a high transmittance of ~97.7%, and etc.[7-8] These unique properties make graphene a key candidate material for many applications such as electronic devices, flexible display, energy devices, advanced composites, barrier material, ink, heat spreader, bio related applications, etc.[9-10]

Despite its excellent properties, wide applications of graphene are not commercially notable until now. Major hurdles for its commercial availability are mass production maintaining proper material quality, that is, technologies considering the production cost as well. Up to now, a large number of methods have been proposed to produce graphene. This method can be divided into two main classes, that is, bottom-up methods and top-down methods. The former depends on the chemical reaction of the molecules to form a covalent bonded two dimensional structure. The latter depends on the separation of the bulk graphite.

The bottom-up methods such as chemical vapor deposition (CVD) and

epitaxial growth are possible to obtain a high quality of graphene with low defects, which is expected to be a good candidate material for the electronic devices.[11-14] However, these substrate-based technology has suffered a limited scale and expensive production costs, which cannot meet the demands of mass production. As a top-down method, graphene produced by liquid phase direct exfoliation of the graphite proved a low-cost, large-scale production of graphene possible.[15] The exfoliation of low-cost graphite to give graphene is one of the most promising way to achieve mass production at a very low cost. Exfoliation methods can be largely divided into chemical exfoliation by strong acids and mechanical exfoliation by physical forces.

The most typical chemical exfoliation method is the modified Hummers processes.[16] This chemical exfoliation requires the involvement of hazardous strong oxidizing reagents (e.g., HNO_3, $KMnO_4$, and/or H_2SO_4) and tedious multistep processes, which give severe damage to the carbon basal plane to introduce a large number of chemical and topological defects. The following reduction reaction also involves hazardous reducing reagents (e.g., hydrazine, $NaBH_4$) with a limited reduction conversion.

On the other hand, the mechanical exfoliation is the separation of the graphite layers to atomically thin sheet through various forces such as mechanical, electrostatic, or electromagnetic forces. In the process, the ideal case is that graphene is peeled off from the bulk graphite layer by layer by overcoming the van der Waals attraction between adjacent layers of graphene. A typical example is a micro-mechanical cleavage (MC). In 2004, a single layered graphene (SLG) was firstly

demonstrated by MC of graphite by a commercial Scotch tape. Although MC is impractical for large-scale applications, it is still the method of choice for fundamental studies. Indeed, the vast majority of basic results and prototype devices were obtained using MC flakes. Thus, MC remains ideal to investigate both new physics and new device concepts.

Besides the peeling-off mechanism, the fragmentation usually simultaneously occurs during exfoliation. The fragmentation by collisions or vertical impact can make large flakes into small ones, but sometimes even destroy the crystalline nature of structures. Therefore, it is expected that to attain high-quality and large-sized graphene, the fragmentation effect should be minimized. However, the fragmentation can promote additional exfoliation, because smaller graphite flakes are easier to exfoliate than larger ones due to the smaller collective van der Waals interaction forces between the layers in smaller graphite flakes.

Among many mechanical exfoliation methods, a ball milling can be a promising candidate for the scalable production of graphene, which uses shear forces to exfoliate graphite flakes. Recently, Jeon et al. suggested an edge functionalized dry ball milling.[17] They dry milled the pristine graphite flakes in for 48 hours in the presence of dry ice, homogenous but much smaller edge-carboxylated graphite grains of the few hundreds nanometer size can be obtained. They claimed the edge-carboxylated graphite is highly dispersible in various solvents and can self-exfoliate into mono and few-layer graphene nanosheets. However, the fragmentation and defects are inevitable during the milling process since high energy collisions among the grinding media cannot be prevented and the long process time of several ten

hours increase the possibility of generating defects.

Besides the above discussed ball milling, the exfoliation methods by the shear force generated from fluid dynamics have a good potential for producing graphene.[18] Graphite flakes can move with the liquid or air flow in a circular container and the centrifugal forces are exerted on the graphene flakes in the opposite direction of drag force by liquid or air flow. Therefore, the flakes experience a shear induced displacement along the wall of the container and are exfoliated efficiently. This mechanism is intrinsically different from that of ball milling in that the fluid dynamics based methods generate directional shear forces by the flow unlike the ball milling uses random directional shear forces and impact forces.

To overcome the existing methods including the described methods above, we propose a high efficient, low cost exfoliation method of graphite to produce graphene using an air jet milling. The compressed air flows generate a vortex to give the graphite flakes directional shear so that the flakes are exfoliated efficiently.

3.2 Experiments

A jet mill grinds graphite flakes by using a high speed jet of compressed air or inert gas such as nitrogen. As described in Fig. 1a, it consists of a cylindrical container, which height is lower than its diameter, where compressed jet is forced into the milling zone through nozzles tangent to the wall of the milling zone. The air jet generates a vortex inside the milling zone along the axis of the cylindrical container. Graphite flakes inside the milling zone are subject to two competing forces, i.e. the centrifugal forces by the graphite flakes traveling in circles and the centripetal forces by the drag from the compressed jet as it flows from the nozzles along the wall to the discharge pot in the center of the mill (Fig. 2). Therefore, the graphite flakes are sorted by their sizes from the wall to the center, that is, small (or light) flakes below a certain size, while larger (or heavier) flakes above the size continue to move in circles, move inward and eventually escape from the mill zone through the discharge pot. Once the small flakes escape from the mill, they are again sorted by their weights and collected from two bottles on the top, i.e. the bottom bottle for the heavier flakes and top bottle for the lighter flakes as described Fig. 1a. As described in Fig. 2a, exfoliation of the graphite flakes is dominated by two different routes, i.e. shear force generated by compressed air flow and the normal force by the centrifugal force and the centripetal force exerted on the graphite layers. The fragmentation of the flakes also occurs mostly by the collisions among the flakes (Fig. 2c) while the flakes are moving in circles with the air flow. Fig. 3 shows the actual air jet milling machine used for this study. The milling zone is made of

Zirconia ceramics with the diameter of 15 cm, which can mill the flakes up to 1 kg at the same time. The air compressor has the pressure ranges from 7.5 to 9.9 kg/cm^2 with the discharge rate of 2050 litters/min, the power of 15 kW, and the tank size of 280 litters.

The natural graphite flakes, which were purchased from Alfa Aesar (#43319, ~10 mesh, 99%), of 51g were fed through the material feeder (Fig. 3d). The applied air pressure kept changed within the ranges from 0.2 to 0.3 MPa while monitoring the collecting bottle to prevent the reverse flow. After the first cycle, which took about 90 minutes, 14 grams of the flakes from the top bottle and 37 grams of the flakes from the bottom bottle were obtained. The amount of the material loss was negligible after the cycle. The first flakes started to be collected from the top bottle only after 4 minutes running of the first cycle. The average size (D_{50}) of the first sample, which was measured by the Fritsch laser particle analyzer, immediately dropped to about 5 microns from about 800 microns of the raw graphite flake with only 4 minutes' run. The average size of the whole 1st cycle sample are almost the same as the first sample after 4 minutes, proving the consistent milling performance. In succession, the 2nd cycle was run for 30 minutes with the flakes collected from the top and bottle after the 1st cycle. The average size and the size distribution of the 2nd cycle did not change much compared to the 1st cycle, saying that the fragmentation dominantly occurs only at the early stage of milling process, that is, the 1st cycle. The 3rd cycle was continuously run for 60 minutes with the flakes obtained from the top bottle after the 2nd cycle. The average size slightly changed from about 5 microns to 3 microns after the 3rd cycle. The changes in the size and morphology of the flakes

are also shown in the SEM images (Fig. 4b), where the marked alphabet represent the stage of the flake samples that the SEM images show respectively.

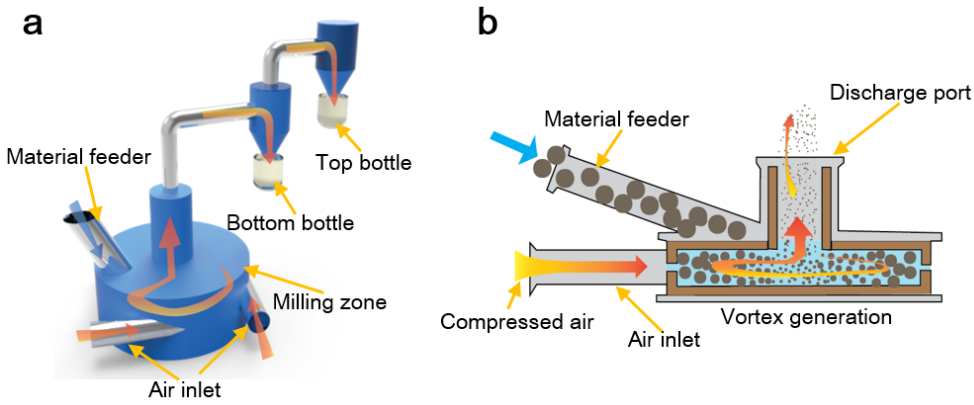

Figure 1. The schematics of exfoliation of graphite using the air jet milling. **a,** The conceptual structure of air jet milling machine. The compressed air is applied in the tangential direction of the milling zone, and the raw graphite is put from the top of the milling zone. The final exfoliated graphene or graphite flakes are obtained from the top and bottom bottles. **b,** The side view of the milling zone. Small flakes enough to stay in the middle escape from the milling zone through the discharge port.

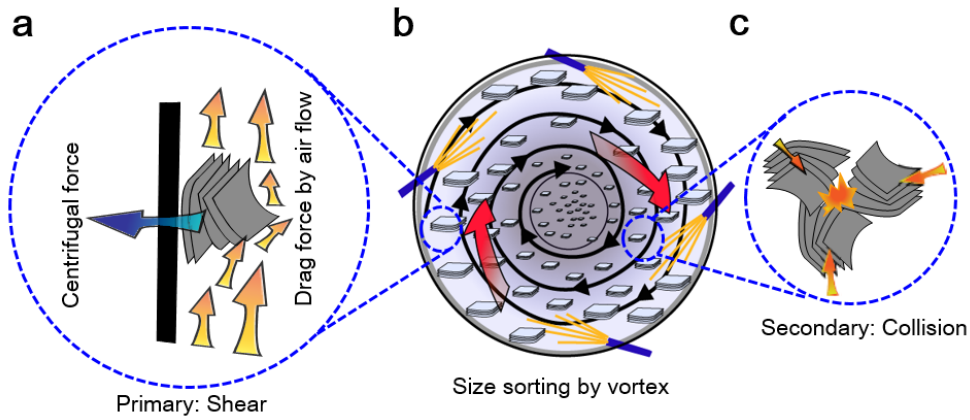

Figure 2. The mechanism of exfoliation and fragmentation of the graphite flakes inside the milling zone. **a,** The normal force is generated by the centrifugal force and the centripetal force exerted on the graphite flakes and the shear force is given by the compressed air flow between the graphite layers. **b,** By the balance between the centrifugal force and the centripetal force, the graphite flakes are sorted by the size and weight from the wall to the center of the mill. **c,** The collisions among the graphite flakes promote the fragmentation of the flakes.

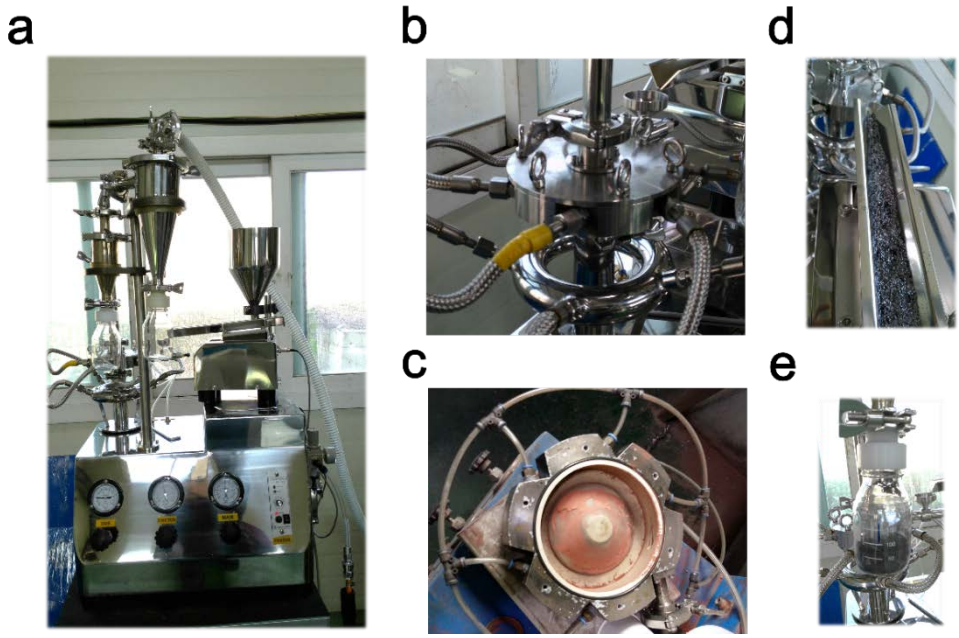

Figure 3. The appearance of the air jet milling machine and its components. **a,** The overall view of the machine. The magnified view of its major components are shown separately from b to e. **b,** The milling zone, where the compressed air are forced into the zone through the nozzles. **c,** The top view inside the milling zone. **d,** The material feeder. **e,** The collecting bottle.

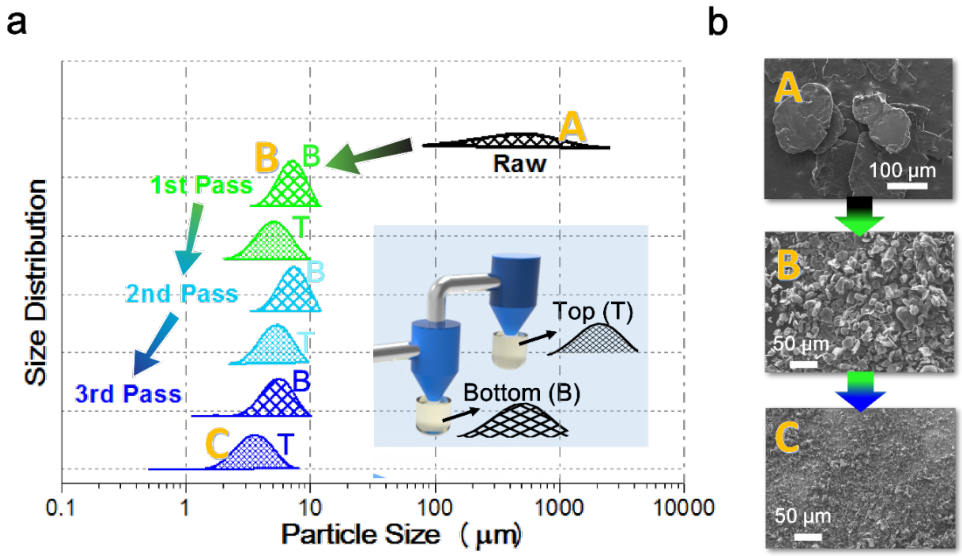

Figure 4. The changes in size and its distribution after three cycle runs of air jet mill. **a,** The profile of size distribution is represented as a hatched closed curve. Thin and thick meshed curves show the distribution of the flakes obtained from the top bottle and the bottom bottle respectively. **b,** SEM images of raw graphite and after each cycle are shown, where the stage is distinguished with alphabets.

3.3 Results and Discussion

FT-IR spectra for the air jet milled samples are obtained as Fig. 5a, where all data are normalized by the intensity of C-C bond. From the spectra, various oxygen configurations are observed as -OH, C=O, C-O, and C-O-C vibration mode, which occur around 3434 cm^{-1}, 1725 cm^{-1}, 1024-1180 cm^{-1}, and 1200 cm^{-1} respectively. In-plane stretching is also observed as the peak around 1629 cm^{-1}, which is the sp^2 hybridized C=C bond. Moreover, the binding energy of C 1s peaks are shifted to the higher binding energy as the cycle repeats, which is caused by the binding energy of C=O around 285.3 eV. It means that the oxygen group (C=O) increases after the air jet mill cycle runs. However, it should be noted that the amount of the shift would not increase much as the jet mill cycle repeats, assuming that the oxygen group increases only when the fragmentation mode is dominant, that is, the first jet mill cycle. Fig. 5c shows the carbon and oxygen percentages calculated from XPS data. The same conclusion can be made from the fact that the oxygen percentage does not increase much as the cycle repeats after the 1^{st} cycle. We can assume that the oxygen functional groups are dominantly bound on the edges of the flakes by fragmentation rather than the defect sites on the basal planes. The jet milled samples show extremely low percentage of oxygen contents about 3 percent even after 3 cycles of jet mills, comparing that the graphene oxide shows high percentage of oxygen concentration of around 30 percent as shown in Fig. 5c.

From the Raman spectra shown in Fig. 6a, the D peaks around 1338 cm^{-1}, indicating defects in graphite and graphene, are negligible as the air jet mill cycle

repeats. G peaks of air jet milled samples are shifted to lower frequency around 1560 cm^{-1} (red shift) compared to the G peak around 1578 cm^{-1} of pristine graphite. The graphite flakes are collided each other and forced by shear while air jet milling, and then are peeled off by layer or broken sometimes,

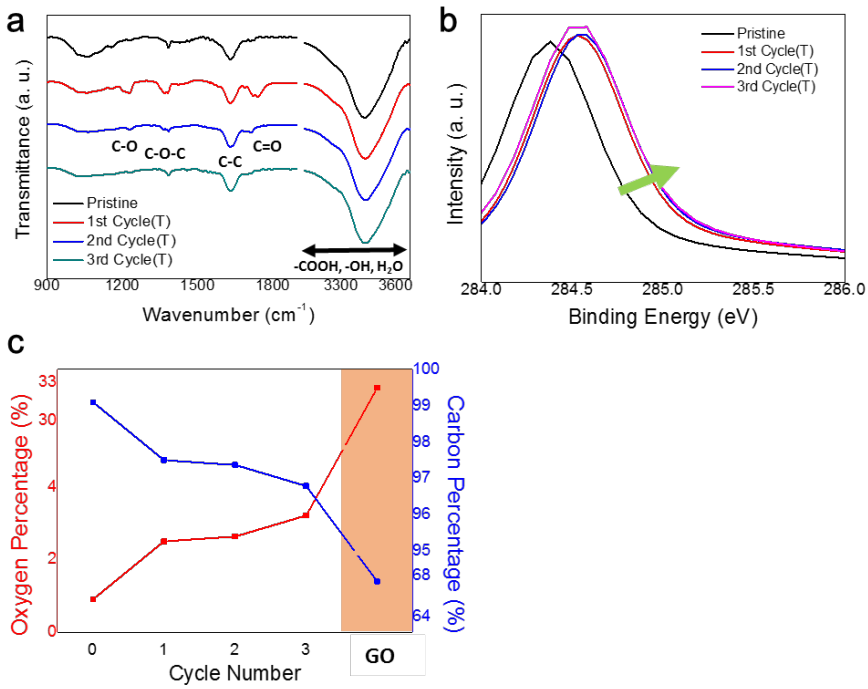

Figure 5. FT-IR analysis and XPS analysis for oxygen concentration. **a,** FT-IR analysis shows the dominant functional groups for the samples from each cycle. **b,** C 1s spectra of XPS analysis. **c**, carbon and oxygen concentration of the air jet milled samples and GO calculated from XPS data.

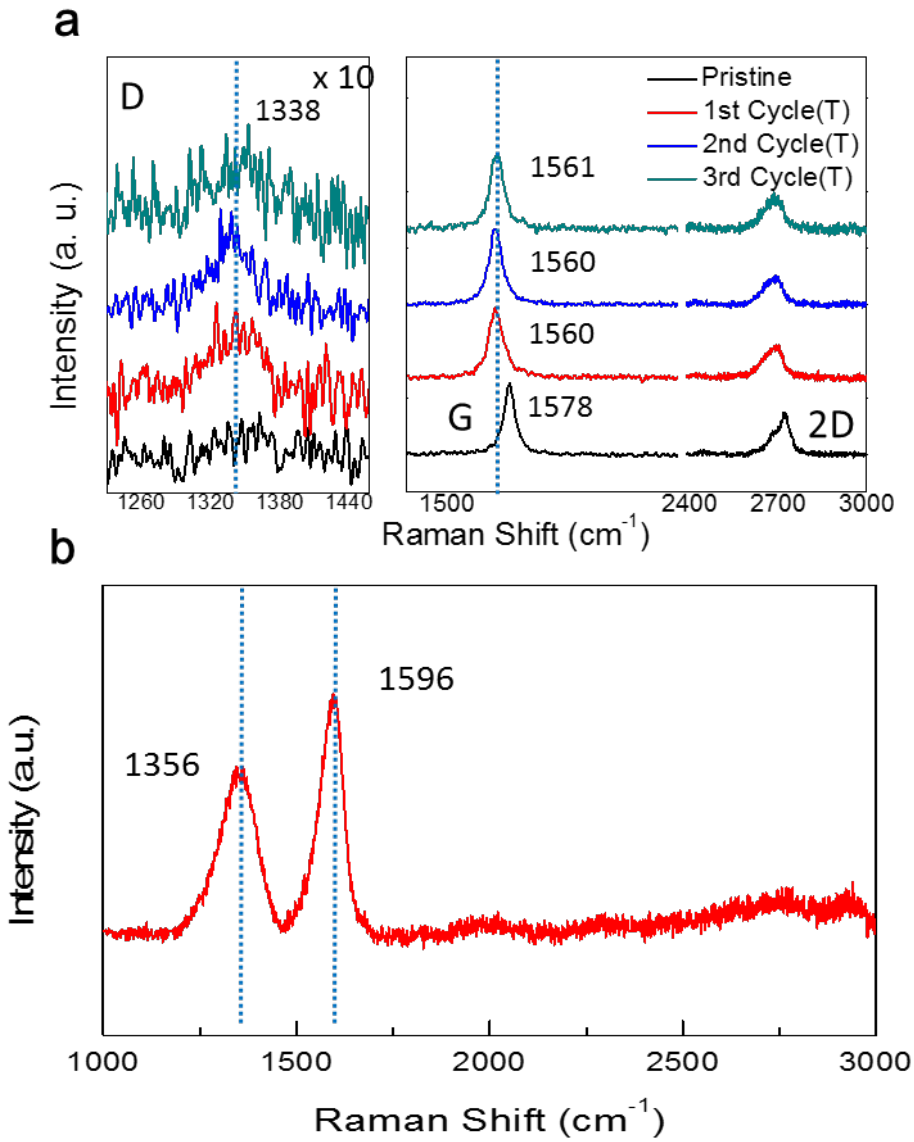

Figure 6. Raman Analysis of the Jet Milled Samples and the Graphene Oxide by typical Hummer's methods. **a,** Raman peaks of jet milled samples. D peaks and the shift of G peaks. All the peaks are normalized by the intensity of G peak. **b,** Raman peaks of GO samples.

resulting in generating disordered graphite layer as sp^3 form on the surface. It gives the decrease in D peak as well as the red shift in G peak. The Raman spectra of GO are quite different from that of the air jet milled graphite in that its D peak and G peak occur around 1356 cm^{-1} and 1596 cm^{-1} respectively. It is known that the carbon turns into amorphous carbon by chemical species during the processes and then the G band is shifted to higher frequency. Compared to the air jet milled graphite, more defects are expected to observe in GO, which is already discussed by XPS data earlier, and are related to make higher intensity in D and G peak.

3.4 Conclusion

The mechanical exfoliation by the air jet mill is very effective and easy to scale up for any industrial application. The proposed method is especially useful for a layered material such as graphite having low interfacial bonding energy between layers so that the layer can be easily exfoliated by the mechanical forces. The raw graphite flakes of average 800 microns in diameter immediately had size reduction to few microns in average diameter within few minutes, which is advantageous considering typical exfoliation method such as ball milling take few tens hours of operation time. During the process, the fragmentation by collision is observed to be more dominant than the exfoliation by shear and normal forces. It is not usually desirable, but small flakes obtained from the air jet mill can enhance the exfoliation efficiency with the help of intercalation agents or further process with minimum amount of chemical promoter. Formation of bonds with undesirable oxygen species kept low up to only few percent even after few successive air jet mill runs, assuming that the defects on the basal plane would not be produced much during the process.

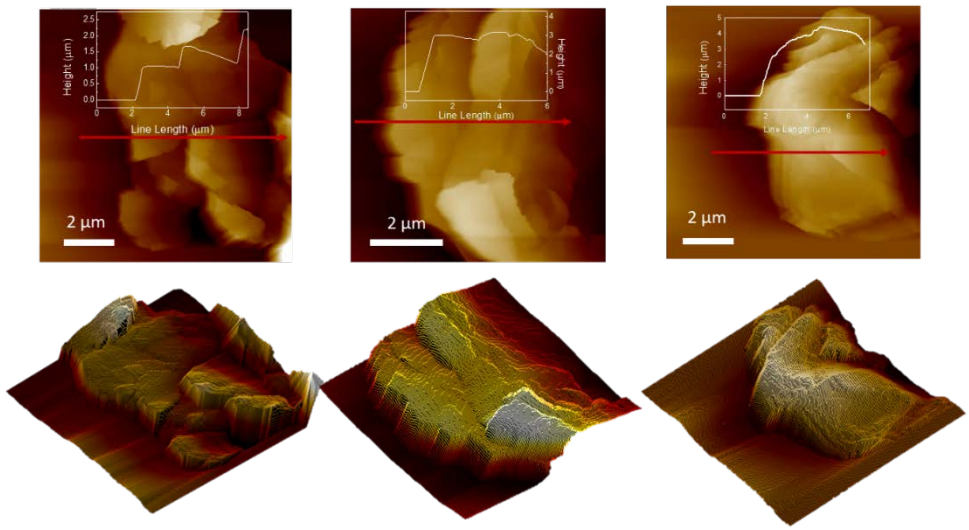

Figure S1. AFM analysis showing the morphology of the flakes. **a,** Graphite flakes from 1st cycle (Top bottle). **b,** Graphite flakes from 2nd cycle (Top bottle). **c,** Graphite flakes from 3rd cycle (Top bottle).

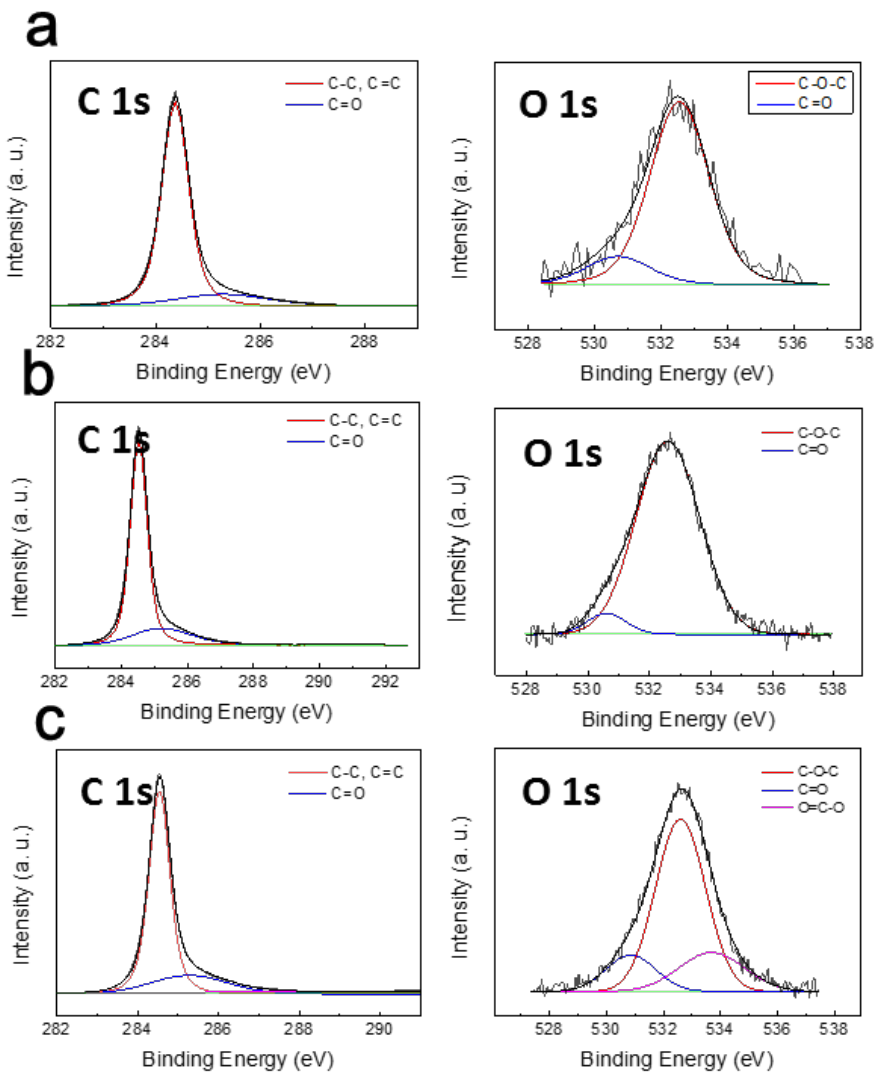

Figure S2. XPS data. **a-c,** C 1s and O 1s peaks from pristine graphite, 1st cycle, and 2nd cycle respectively.

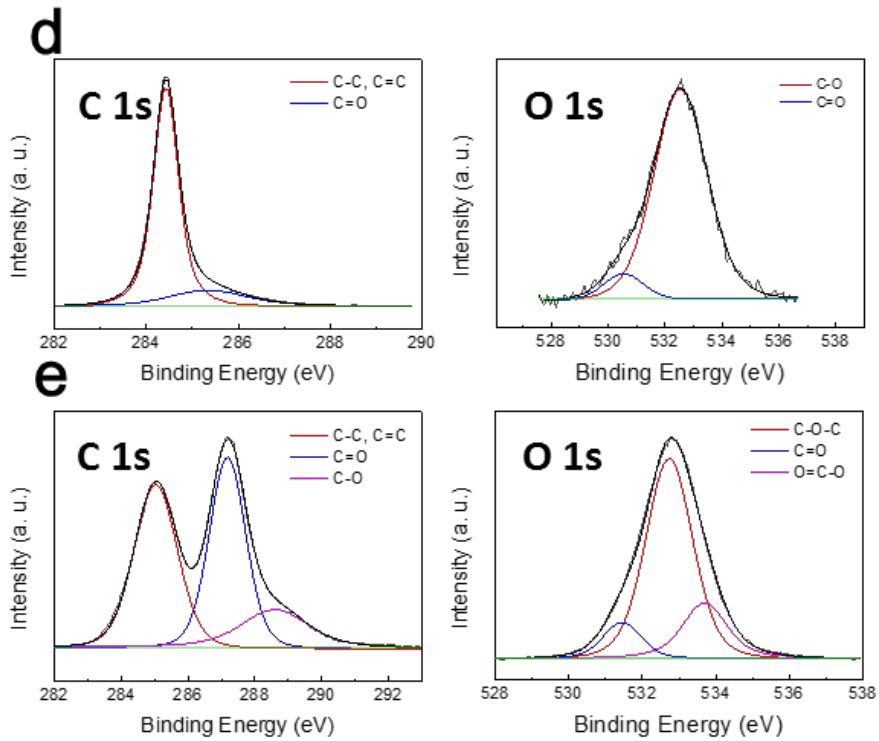

Figure S2. XPS data. **d-e,** C 1s and O 1s peaks from 3rd cycle and Graphene oxide respectively.

3.5 References

[1] K. S. Novoselov, A. K. Geim, S. Morozov, D. Jiang, Y. Zhang, S. Dubonos, I. Grigorieva and A. Firsov, *Science*, **2004**, 306, 666–669.

[2] C. Lee, X. Wei, J. W. Kysar and J. Hone, *Science*, **2008**, 321, 385–388.

[3] A. S. Mayorov, R. V. Gorbachev, S. V. Morozov, L. Britnell, R. Jalil, L. A. Ponomarenko, P. Blake, K. S. Novoselov, K. Watanabe, T. Taniguchi and A. K. Geim, *Nano Lett.*, **2011**, 11, 2396–2399.

[4] F. Liu, P. Ming and J. Li, *Phys. Rev. B: Condens. Matter Mater. Phys.*, **2007**, 76, 064120.

[5] A. A. Balandin, *Nat. Mater.*, **2011**, 10, 569–581.

[6] A. A. Balandin, S. Ghosh, W. Bao, I. Calizo, D. Teweldebrhan, F. Miao and C. N. Lau, *Nano Lett.*, **2008**, 8, 902–907.

[7] J. S. Bunch, S. S. Verbridge, J. S. Alden, A. M. van der Zande, J. M. Parpia, H. G. Craighead and P. L. McEuen, *Nano Lett.*, **2008**, 8, 2458–2462.

[8] R. R. Nair, P. Blake, A. N. Grigorenko, K. S. Novoselov, T. J. Booth, T. Stauber, N. M. Peres and A. K. Geim, *Science*, **2008**, 320, 1308.

[9] K. S. Novoselov, V. I. Fal'ko, L. Colombo, P. R. Gellert, M. G. Schwab and K. Kim, *Nature*, **2012**, 490, 192–200.

[10] T. R. Nayak, H. Andersen, V. S. Makam, C. Khaw, S. Bae, X. Xu, P.-L. R. Ee, J.-H. Ahn, B. H. Hong, G. Pastorin and B. Özyilmaz, *ACS Nano*, **2011**, 5, 4670–4678.

[11] K. S. Kim, Y. Zhao, H. Jang, S. Y. Lee, J. M. Kim, K. S. Kim, J. H. Ahn, P. Kim, J. Y. Choi, and B. H. Hong, *Nature*, **2009**, 457, 706-710.

[12] S. Bae, H. Kim, Y. Lee, X. F. Xu, J. S. Park, Y. Zheng, J. Balakrishnan, T. Lei, H. R. Kim, Y. I. Song, Y. J. Kim, K. S. Kim, B. Ozyilmaz, J. H. Ahn, B. H. Hong, and S. Iijima,, *Nature Nanotechnology*, **2010**, 5, 574-578.

[13] X. Li, W. Cai, J. An, S. Kim, J. Nah, D. Yang, R. Piner, A. Velamakanni, I. Jung, E. Tutuc, S. K. Banerjee, L. Colombo and R. S. Ruoff, *Science*, **2009**, 324, 1312–1314.

[14] W. Strupinski, K. Grodecki, A. Wysmolek, R. Stepniewski, T. Szkopek, P. E. Gaskell, A. Gruneis, D. Haberer, R. Bozek, J. Krupka and J. M. Baranowski, *Nano Lett.*, **2011**, 11, 1786–1791.

[15] Y. Hernandez, V. Nicolosi, M. Lotya, F. M. Blighe, Z. Sun, S. De, I. T. McGovern, B. Holland, M. Byrne, Y. K. Gun'Ko, J. J. Boland, P. Niraj, G. Duesberg, S. Krishnamurthy, R. Goodhue, J. Hutchison, V. Scardaci, A. C. Ferrari and J. N. Coleman, *Nat. Nanotechnol.*, **2008**, 3, 563–568.

[16] W. S. Hummers and R. E. Offeman, *J. Am. Chem. Soc.*, **1958**, 80, 1339–1339.

[17] I. Y. Jeon, H. J. Choi, S. M. Jung, J. M. Seo, M. J. Kim, L. Dai, and J. B. Baek , *J. Am. Chem. Soc.*, **2013**, 135, 1386−1393

[18] I. Y. Jeon, Y. R. Shin, G. J. Sohn, H. J. Choi, S. Y. Bae, J. Mahmood, S. M. Jung, J. M. Seo, M. J. Kim, D. Wook Chang, L. Dai and J. B. Baek, *Proc. Natl. Acad. Sci. U. S. A.*, **2012**, 109, 5588–5593.

[19] K. R. Paton, E. Varrla, C. Backes, R. J. Smith, U. Khan, A. O'Neill, C. Boland, M. Lotya, O. M. Istrate, P. King, T. Higgins, S. Barwich, P. May, P. Puczkarski, I.

Ahmed, M. Moebius, H. Pettersson, E. Long, J. Coelho, S. E. O'Brien, E. K. McGuire, B. M. Sanchez, G. S. Duesberg, N. McEvoy, T. J. Pennycook, C. Downing, A. Crossley, V. Nicolosi and J. N. Coleman, *Nat. Mater.*, **2014**, 13, 624–630.

APPENDIX

A. List of Publications

[1] T. Choi*, S. J. Kim* et al. "Roll-to-roll Continuous Patterning and Transfer of Graphene via Dispersive Adhesion" *Nanoscale* 7, 7138-7142 (2015). (Hot Paper)

[2] S. J. Kim*, T. Choi* et al. "Ultra-Clean Patterned Transfer of Single-Layer Graphene by Recyclable Pressure Sensitive Adhesive Films" *Nano Letters* 15, 3236–3240 (2015).

[3] Choi, Taejun; Kim, Sang Jin; Park, Subeom; Hwang, Taekyong; Jeon, Youngro; Hong, Byung Hee; "Roll-to-roll synthesis and patterning of graphene and 2D materials" *2015 IEEE International Electron Devices Meeting (IEDM)* 27.7. 1-27.7. 4

국문초록

2000년대 초반부터 진행된 많은 연구들을 통해서 전기적, 기계적, 광학적, 열적 등의 많은 분야에서의 그래핀의 우수한 특성들이 밝혀졌고 이에 유연소자, 에너지, 광학, 차폐소재 등 많은 분야에서 핵심 소재로서 응용을 기대해 왔으나 실제 산업에서의 활용은 제한되어 있었다. 주요한 원인으로는 그래핀의 생산 이후의 제품으로 실제 적용되기까지 특성이 저하되는 문제와 함께 산업적으로 응용 가능할 수준의 경제적인 대량생산의 방법의 부재이었다.

본 학위논문은 그래핀의 산업적 응용을 가능하게 하는 대면적 그래핀 전사 및 패터닝의 방법과 함께 그래핀의 경제적 대량 생산이 가능한 방법을 다뤘다. 이에 따른 본 논문의 구체적인 목표는 다음과 같다. (1) 화학적 증착법에 의한 대면적으로 합성된 그래핀을 특성 변화를 최소화하며 목표 기판에 연속공적으로 전사 및 패터닝하는 방법을 제시하는 것이다. (2) 물리적인 박리법에 의해 불필요한 원소들의 결합을 최소화하며 경제적이고 효율적인 그래핀의 대량 생산법을 제시하는 것이다.

본 논문의 주요 결과는 다음과 같다. 첫째, 낮은 표면에너지를 가지는 실리콘 기반의 점착 필름을 응용하여 롤투롤 공정에 적용 가능한 그래핀 전사 및 패터닝 방법을 보여주었다. 제시한 PSAF 필름은 반복사용이 가능하며 기존의 보편적인 전사방법으로 사용되던 PMMA법이나 열전사필

름(TRT)에 비해 잔유물이 적어 그에 따른 의도되지 않은 도핑효과나 전자이동도의 감소 같은 특성의 변화를 최소화 할 수 있었으며 롤투롤 연속 공정에 적용시 동시 패터닝과 전사가 가능하였다.

둘째, 에어젯밀에 의한 그래파이트의 물리적 박리 방법은 기존의 방법들에 비하여 고효율의 박리 및 사이즈 감소를 가능하게 하였고 그 원인은 압축공기의 회전에 의해 발생되는 원심력에 의해 그래파이트 입자가 회전하면서 발생하는 전단력이며 또한 입자간의 충돌에 의해 야기되는 사이즈 감소에 의한 것이었다. 기존의 수십시간 내지는 수일이 소요되는 방법들에 비해 수분~수시간내의 빠른 시간내의 박리 및 분쇄가 가능하였다. 하지만 작용되는 전단력에 의한 박리보다는 입자간의 충돌에 의한 사이즈 감소가 더 주도적으로 발생하여 이에 대한 추가적인 연구가 필요하다.

본 연구의 결과들은 서두에서 언급한 것과 같이 그래핀을 산업에 응용하는데 있어서 유용하게 사용될 수 있으며 그래핀의 우수한 특성들이 실제 제품에서 적용되는 것을 앞당길 수 있을 것으로 기대한다.

주요어: 그래핀, 대면적 전사, 대면적 패터닝, 기계적 박리, 대량 생산

학번: 2013-30095